HUMAN STABILITY AND THE LIKELIHOOD OF FALLING: A COMPARISON OF WALKING AND SKIING LOCOMOTION

by

Andrew Peter Vogt

A dissertation submitted to the faculty of
The University of Utah
in partial fulfillment of the requirements for the degree of

Doctor of Philosophy

Department of Mechanical Engineering

The University of Utah

December 2013

The University of Utah Graduate School

STATEMENT OF DISSERTATION APPROVAL

The dissertation of **Andrew Peter Vogt**

has been approved by the following supervisory committee members:

Stacy Bamberg	, Chair	**10/30/2013** Date Approved
Donald Bloswick	, Member	**10/30/2013** Date Approved
Larry DeVries	, Member	**10/30/2013** Date Approved
Bo Foreman	, Member	**1/1/2013** Date Approved
Andrew Merryweather	, Member	**10/30/2013** Date Approved

and by **Tim Ameel**, Chair/Dean of

the Department/College/School of **Mechanical Engineering**

and by David B. Kieda, Dean of The Graduate School.

ABSTRACT

This thesis analyzed biped stability through a qualitative likelihood of falling and quantitative Potential to Fall (PF) analysis. Both analyses were applied to walking and skiing to better understand behaviors across a wider spectrum of bipedal gaits. For both walking and skiing, two types of locomotion were analyzed. Walking studies compared normal locomotion (gait) to an unexpected slip. Skiing studies compared wedge style locomotion (more common to beginning and intermediate skiers) to parallel style locomotion (more common to advanced and expert skiers).

Two mediums of data collection were used. A motion capture laboratory with stereographic cameras and force plates were used for walking studies, and instrumented insoles, capable of force and inertial measurement, were used for skiing studies.

Both kinematics and kinetics were used to evaluate the likelihood of falling. The PF metric, based on root mean squared error, was used to quantify the likelihood of falling for multiple subjects both in walking and skiing. PF was based on foot kinematics for walking and skiing studies. PF also included center of pressure for skiing studies. The PF was lower for normal gaits in walking studies and wedge style locomotion for skiing studies.

This is dedicated to the importance of living a happy life and pursuing passion.

CONTENTS

LIST OF FIGURES

ACKNOWLEDGMENTS

I would like to graciously thank Luke, my wonderful husband, who has supported and grown with me throughout this process; Peter, my dad, who made me have a love for life; Allie, my mom, who convinced me never to give up and who I could talk to for hours on end; Lauren, my sister, who stands up for me and is my advocate in childish humor; Fred Moore, a great friend, who has inspired this work with his will to overcome physical challenges; and Stacy Bamberg, my advisor and friend, who has never turned me away and helped my accomplish my goal.

A special thanks to Snowbird Ski and Summer Resort in Snowbird, Utah for graciously allowing cost-free use of their facilities. Also, a special thanks to Snowbird Mountain School for their generous intellectual support.

CHAPTER 1

INTRODUCTION

Motivation

Human upright posture is analogous to the inverse pendulum problem. It is practically impossible to avoid falling without accurately knowing posture and providing correcting force inputs. Humans use sensory, (nerves, eyes, ears, etc.), cognition (the brain), and actuation (muscles) systems to regulate posture and balance. If any systems are compromised, then the likelihood of falling increases.

Fall may arise from a variety of factors, including altered abilities due to disabilities, disease, or age. Pathologic gait leads to functional impairment [1], which will affect sensory, cognition, or actuation systems. Since balance is dependent on all three systems, if any are compromised, then balance is compromised. Loss of balance leads to increased likelihood of falling [2, 3]. While pathologic gait and locomotion amplify the effect of disturbances, this still helps to understand how disturbances lead to increased likelihood of falling. Falls may also arise from a destabilizing event, which is an environmental disturbance. This is usually an unexpected event, such as a slip or trip, that increases the likelihood of falling. One of the purposes of this work is to help understand falls resulting from any of these factors.

In this work, the *likelihood of falling* is used as a qualitative description of falling probability. The *Potential to Fall* metric quantifies falling probability but is also used to describe the likelihood of falling.

Data Collection

Diverse Locomotion Testing

Locomotion describes any means of self-propulsion. Gait specifically applies to situations where feet generate propulsive or stabilizing reaction forces such as stand-

ing, walking, or running. Aside from gait, humans have discovered and created many other types of locomotion such as climbing, cycling, skating, and skiing.

The primary focus on this work is understanding the factors that increase the likelihood of falling. There can be very large deviations between types of locomotion, which makes it difficult to generalize human locomotion. In this work, two very different types of human locomotion were compared: walking and skiing.

Both walking and skiing studies compared low to high likelihood of falling scenarios. The walking study compared normal gait to unexpected slipping gaits and the skiing study compared wedge style to parallel style locomotion. The unexpected slip of the walking study caused a destabilizing disturbance, which led to a higher likelihood of falling.

The likelihood of falling problem for skiing is challenging because, unlike walking, normal locomotion is not clearly defined. One of the first learned styles of skiing is wedge style (WS). WS affords relatively easier balancing and speed control due to a wide base of support and greater resistance to forward movement, respectively. As skiers become more familiar with WS, their sensory, cognition, and actuation improve and they are able to apply more advanced styles, namely parallel style (PS), which requires refined balance. PS can be therefore treated as a skiing locomotion with increased potential to fall when compared to WS.

Subject Demographics

For both walking and skiing tests, only healthy subjects were used. The walking tests had 14 original subjects; the 4 analyzed here experienced appreciable slip. The skiing test had 12 original subjects; the 9 analyzed here had complete data sets collected.

Testing and Data Capture

Due to the complex nature of human motion, selecting appropriate means of data collection was important for obtaining meaningful results. This research involved two types of locomotion: walking and skiing. Walking studies were conducted in a motion capture laboratory because a normal walking environment could effectively be simulated. This particular laboratory was equipped with a stereographic camera

system and four force plates to capture complete walking dynamics. All analyzed subjects made unique contact between each foot and a force plate over four steps. Subjects were told that the force plates would be dry for the first few tests. Without the subjects' knowledge, the third force plate was coated with a water-glycol solution to initiate an unexpected slip.

A laboratory setting was not suitable for skiing studies because it was extremely difficult, and expensive, to mimic the environment. Specially designed instrumented insoles (Fig. 1.1) measured force toward the toe and heel, and midfoot 6-Degree of Freedom (DOF) inertial measurement. These insoles made it possible to use the natural environment to conduct this study.

Three types of tests were conducted in the skiing study. All tests were conducted on gentle-sloped beginner terrain. The first tested the skier's baseline abilities and habits. During this study, every skier was asked to ski normally while making turns. The next two tests were conducted in a course using evenly spaced cones to initiate turning. These two tests examined the skier's ability to navigate a marked course while performing WS and PS skiing.

Research Hypothesis, Specific Aims, and Supporting Chapters

The research hypothesis is as follows: *Center of Pressure (COP) and kinematic marker trajectories change as the likelihood of falling changes in human walking gait and human skiing gait.* This was investigated through the following specific aims:

- Aim 1: Likelihood of falling while walking was investigated using kinematic hip and foot markers, captured from a stereographic cameras system, and kinetic changes in COP, captured from 6-DOF force plates (under each foot). This was investigated through an analysis of the dataset of normal versus unexpected slipping gaits collected with our collaborator, Dr. Kurt Beschorner [4].

- Aim 2: Likelihood of falling while skiing was understood using foot kinematics, from Inertial Measurement Units (IMUs), and the change in COP, from Force Sensitive Resistors (FSRs), under each foot. Both IMUs and FSRs are embedded within instrumented insoles, as shown in Fig. 1.1. Two basic groups are analyzed: expert skiers, and intermediate skiers where intermediate skiers

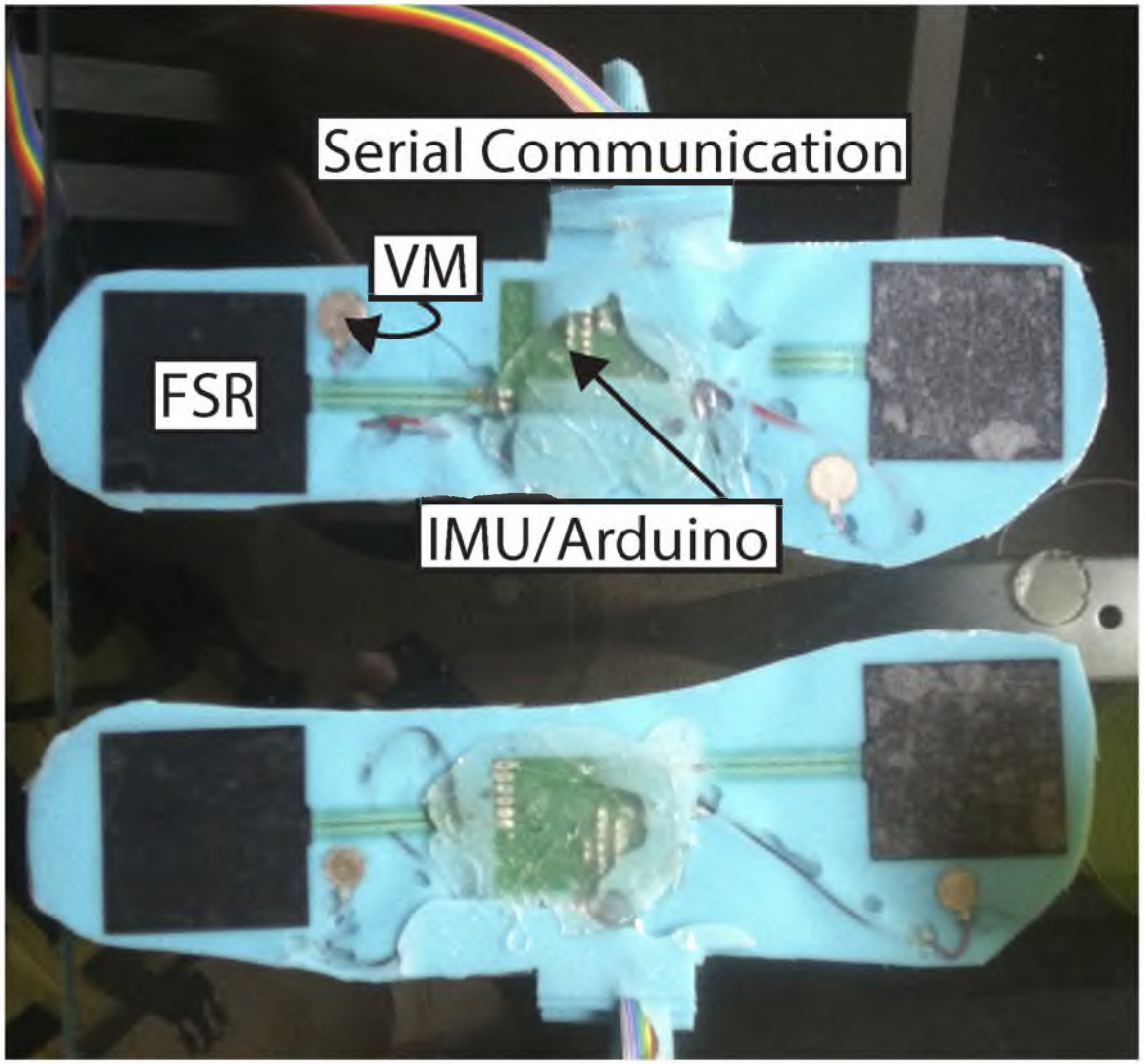

Figure 1.1: Photograph of instrumented insoles after pouring the mold. In each insole, there are two Force Sensitive Resistors (FSR), two Vibrotactile Motors (VM), an Inertial Measurement Unit (IMU), and an Arduino Microcontroller. The Arduino communicates using serial communication.

assume to have an overall higher skiing likelihood of falling. Two types of skiing locomotion were analyzed, WS and PS, with WS amused to have a lower skiing likelihood of falling compared to PS.

In all studies, there was no indication that a fall occurred. However, there are general indicators of a decrease in balance. Many researchers have found that correcting balance perturbations are critical to reduce the risk of falling [2, 3]. Conversely, increased balance perturbations introduced through the unexpected slip and change

from WS to PS skiing are expected to increase the likelihood of falling. Inherited and destabilizing disturbances are analyzed, but both indicate a loss of balance and therefore an increase in the likelihood of falling.

Aim 1 is addressed in Chapters 2 and 3, and Aim 2 is addressed in Chapters 4 and 5. Concluding statements are presented in Chapter 6.

References

[1] J. Perry, *Gait Analysis*. Thorofare, NJ: SLACK Incorporated, 2010.

[2] B. E. Maki, K. M. Sibley, S. B. Jaglal, M. Bayley, D. Brooks, G. R. Fernie, A. J. Flint, W. Gage, B. A. Liu, W. E. McIlroy, A. Mihailidis, S. D. Perry, M. R. Popovic, J. Pratt, and J. L. Zettel, "Reducing fall risk by improving balance control: Development, evaluation and knowledge-translation of new approaches," *Journal of Safety Research*, vol. 42, no. 6, pp. 473 – 485, 2011, ¡ce:title¿Elderly Falls¡/ce:title¿. [Online]. Available: http://www.sciencedirect.com/science/article/pii/S0022437511001150

[3] Y.-C. Pai, J. Wening, E. Runtz, K. Iqbal, and M. Pavol, "Role of movement stability in reducing slip-related balance loss and falls among older adults," Piscataway, NJ, USA, 2003//, pp. 253 – 6, movement stability;slip-related balance loss;body center of mass;mathematical models;mathematically predicted dynamic stability;. [Online]. Available: http://dx.doi.org/10.1109/CNE.2003.1196806

[4] P. Hur and K. Beschorner, "Investigating the link between kinematic deviations and recovery response to unexpected slips," in *American Society of Biomechanics Conference*, 2012.

CHAPTER 2

SLIP, STABILITY, AND THE POTENTIAL TO FALL IN WALKING BIPEDAL SYSTEMS

Introduction

This chapter discusses the complex problem of stability in walking bipeds. There are two conference papers included in this chapter, both of which are aimed toward identifying stability. In the first paper, a pilot study of one subject, slipping stability of the foot was evaluated by correlating slip velocity (the velocity of the contact point relative to the ground) to traction force, and compared to slipping stability of automotive traction control systems. The second paper, established *Potential to Fall* as a quantifiable metric associated with human stability.

Traction Force Characterization of Human Bipedal Systems

The following paper is reprinted with permission form Andrew Vogt, Lucas Lincoln, Stacy Bamberg, and Mark Minor, *Traction Force Characterization of Human Bipedal Systems*, 2010 Intelligent Robots and Systems (IROS), October 2010.

The 2010 IEEE/RSJ International Conference on
Intelligent Robots and Systems
October 18-22, 2010, Taipei, Taiwan

Traction Force Characterization of Human Bipedal Motion

Andrew Vogt, Lucas Lincoln, Stacy J. Morris Bamberg, *Member, IEEE,* and Mark Minor, *Member, IEEE*

***Abstract*— Traction estimation and control, common in the automotive industry, have yet to be extended to human bipedal motion. This paper presents a novel metric for slip and traction optimization using the partial derivative of a traction force estimate to slip velocity. The metric is verified computationally using an existing dynamic mode and experimentally using a multi-camera motion capture system.**

I. Introduction

Slip is a difficult uncertainty which complicates effective operation of many dynamic systems. Slippery surfaces are found in 66% of fall-related hip fractures [1]. Realizing issues caused by slip, the automotive industry has made strides to both model and control slip and traction. Slip can be visualized as the relative velocity of the contact point between two surfaces. Traction, on the other hand, is the force between the two surfaces caused by slip. Both anti-lock braking systems (ABS) and traction control systems (TCS) modulate slip and attempt to control traction forces, with the goal of improving driver safety.

Although these systems work well for an average driver, they are incapable of maximizing traction forces. Experienced drivers, similar to athletes, have proprioception acutely attuned to their vehicular-terrain interaction; this provides an ability to modulate slip thereby improving traction forces beyond the capability of typical ABS or TCS systems. This paper illustrates that techniques to improve traction force by modulating slip can be readily extended to human bipedal motion. Important applications include rehabilitation, humanoid and bio-inspired robotics, and smart prosthetics.

Aside from maximizing traction forces, a valuable side-effect of these techniques is they are attuned to human proprioception. This could help individuals gain proprioceptive abilities similar to athletes. Specifically, this benefits individuals suffering from depleted tactile feedback. In addition, this research can help study why falls occur in patients with limited motor skills; this includes the elderly and Parkinson's disease patients.

The main objectives of this paper are to identify a human slip metric and illustrate the potential to maximize human traction force. The first critical step in this process is identifying a traction model.

The automotive industry bases many traction controllers on the causal relationship between wheel slip (λ) and tyre traction coefficient (μ), as illustrated for many surfaces in Fig. 1. λ is a non dimensional unit (further explained on the next page) where λ=0 and λ=1 mean no slip and full slip are occurring, respectively; μ is the standard Coulomb friction relationship. We hypothesize that a human exhibits a similar causal relationship between slip and traction force.

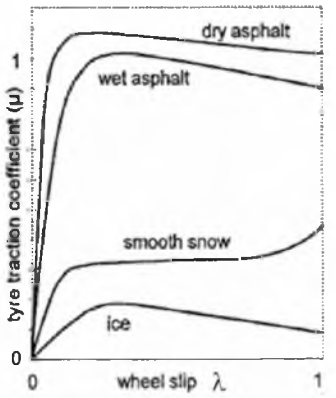

Fig. 1: Slip curves for typical surfaces [2, 3].

For most surfaces, the slip-traction curve (also called the 'slip curve' for simplicity) has the same characteristics: increasing λ from 0 causes μ to increase to a local maximum, where continuing to increase λ causes μ to decrease.

Problematically, the slip curve is highly variable and must be determined empirically for any change in surface conditions. Although we cannot determine all parameters of the curve with accuracy, this paper shows how we can identify the critical parameters needed for human traction control.

The rest of this paper is organized as follows: Section II contains pertinent background information illustrating the contributive nature of our research, section III explains how we can maximize traction force online, section IV presents results, section V discusses significant successful issues, section VI explores future work, and section VII reiterates this paper's important points and presents final concluding remarks.

II. Background

Based on our prior work [4], a standard slip curve is commonly used to determine the relationship between wheel

Manuscript received March 11, 2010. This work was supported in part by NSF Grant No DGE-0654414

Andrew Vogt is with the Department of Mechanical Engineering, University of Utah, Salt Lake City, UT 84112 USA. (phone: 801-587-9018, e-mail: vogt@eng.utah.edu).

Lucas Lincoln is with the Department of Mechanical Engineering, University of Utah, Salt Lake City, UT 84112 USA. (phone: 801-587-9018, e-mail: lucas.lincoln@utah.edu).

Stacy Bamberg is with the Department of Mechanical Engineering, University of Utah, Salt Lake City, UT 84112 USA. (phone: 801-587-9018, e-mail: sjm.bamberg@utah.edu).

Mark Minor is with the Department of Mechanical Engineering, University of Utah, Salt Lake City, UT 84112 USA. (e-mail: minor@mech.utah.edu).

slip and traction force. [4] was inspired by the European Delft-Volvo collaboration, led by Pacejka in the early 90's, which established the physics-inspired "magic tyre formula" [5]. The advantages of this model are its high adaptability to varying terrain. While suited for hard surfaces, such as pavement [6], experimental data shows applicability of these fundamental models to other surfaces such as sandy loam [7] as well as snow and ice [8]. Typical analytical models, on the other hand, are often so intensive that they are used offline in Finite Element Methods (FEM) or vehicle dynamics analysis. Striving for simplicity and computational speed, some researchers rely upon empirical models for traction characterization, but include specific analytic terms to better improve accuracy [9-11]

Perhaps the greatest application of this research is helping those with limited tactile feedback. Guillian Barré patients suffer from a acute peripheral neuropathy hindering their ability to sense or actuating their peripherals [12]. Research has already shown the benefits of improving prosthetics with pressure sensing devices [13], but our goal is to provide patients more complete sensing capabilities by giving them a sense of traction.

At slow gait speeds, self-selected by older adults, falls caused by slips typically impact the hip area, risking fracture of the femur [14]. Dynamic posture depends on proprioceptive, vestibular, and visual sensory inputs, and is affected by perturbations [15] and shaped by an internal representation of body dynamics [16]. Although the coefficient of friction between the foot and walking surface is important, foot kinematics of the foot at heel strike are also critical [17]. Our traction control research would allow us to further evaluate impacts on foot traction in human stability.

III. Methods

We develop human slip principles analogous to established wheeled slip principles as follows:

A. Wheel-Based Definition of Slip

The methods developed by our research are aimed at identifying critical parameters of the slip curve. Parameters defining the point of maximum force (μ_{max}) and corresponding slip (λ_{max}) are arguably the most important because they segregate the region of stable monotonically increasing traction force given increasing slip (when $0 < \lambda < \lambda_{max}$) and the region of unstable monotonically decreasing traction force given increasing slip (when $\lambda_{max} < \lambda < 1$).

As prior stated, using the slip curve to develop traction control has primarily been considered for wheeled vehicles. To understand how slip is defined for human motion then it is useful to consider first the definition for wheeled vehicles. Slip for wheeled vehicles is simply a comparison of translational to rotational speed:

$$\lambda = 1 - \frac{v}{\omega \cdot r_w} = \frac{\omega - v/r_w}{\omega}, \text{ where } 0 < \lambda < 1. \quad (1)$$

In (1), ω is angular speed, v is translational speed, and r_w is the radius of the wheel. The problem, as demonstrated by our prior research [4], is that mobile robots have ill-posed λ because they travel at slow speeds. This happens because as angular velocity approaches zero, λ approaches a singularity. We therefore define a new metric, slip velocity (α), such that

$$\alpha = \omega - v/r_w, \quad (2)$$

which eliminates the denominator of (1).

A *wheel with no slip* exhibits $\alpha = 0$, therefore

$$\omega_{NS} = v/r_w, \quad (3)$$

where ω_{NS} is the no-slip angular speed (i.e. angular speed *only* contributing to forward motion).

In the event of *pure wheel slip*

$$v = 0 \text{ and } \omega = \omega_s \Rightarrow \alpha = \omega_s \quad (4)$$

where ω_S is the amount of angular speed that does not contribute to translational speed. In pure slip, therefore, the slip velocity is exactly equal to ω_S.

In (2), ω can be replaced with the addition of ω_S and ω_{NS} as follows

$$\alpha = \omega_{NS} + \omega_S - v/r_w. \quad (5)$$

Then, (3) can be substituted into (5) which results in

$$\alpha = \omega_s = v_s / r_w \quad (6)$$

v_S is the tangential velocity contributing *only to* wheel slip and has *absolutely no* contribution to translational motion. We can re-define translational slip velocity as

$$\alpha_{TRANS} = v_s = \alpha r_w \quad (7)$$

Because r_W does not change, α and α_{TRANS} change linearly with respect to each other. The greatest result of (7) is a slip velocity metric independent of ω, linearly related to α, and most importantly able to be applied directly to human motion.

B. Human-Based Translation Slip Velocity

Slip for bipedal motion could be defined very similarly to (6) where r_W is approximately equal to the distance between the ankle and hip (i.e. the distance to the center of rotation). Nevertheless it remains desirable to have a metric independent of r_W because gait could significantly alter r_W deeming (6) unreliable. (7)'s independence of r_W, on the other hand, makes it an ideal slip metric.

Though α_{TRANS} is mathematically different than λ,, our experiments show that the general shape of the human-based slip curve remains intact in comparison to Fig. 1. Fig. 2 shows plots the slip curves (shear force v. α_{TRANS}) of both heel-contact (HC) and toe-release (TR) data for normal and induced slip gaits. Their similarity to the automotive industry's λ v. μ curves (Fig. 1) offer justification in applying wheel vehicle traction principles to bipedal motion.

In addition, α is more tractable than λ because it compares ω and v on range from 0 to ω rather than a range restricted between 0 and 1. This is a particularly nice extension for humans because our abundance of senses make it difficult to

purely isolate relative slip. It is shown in subsection *C* that is just as usable as for determining critical slip curve parameters.

C. Critical Slip Curve Parameters

Recall, as discussed previously, there are two distinct regions on the slip curve: One where traction force is monotonically increasing; and one where it is decreasing. We can identify our location on the slip curve by its slope, defined as: $\beta = \partial\mu / \partial\lambda$ In terms of slope and stability,

$$\begin{aligned} &\beta > 0 \text{ (stable slip)} \\ &\beta = 0 \text{ (marginally stable slip)} \\ &\beta < 0 \text{ (unstable slip)} \end{aligned} \tag{8}$$

Likewise, using our new slip metric α, we can define a analogous slope:

$$\hat{\beta} = \frac{\partial \tau(t)}{\partial \alpha(t)} = \frac{\partial \tau(t)}{\partial t}\left(\frac{\partial \alpha(t)}{\partial t}\right)^{-1} \tag{9}$$

effectively replacing β for characterizing stability. In (9), τ represents an estimation of traction force, which can be determined by force sensors or observer systems.

If we assume the radius of rotation of the leg is constant, then $\partial\alpha_{TRANS} = \partial\alpha$. This affords the benefit of using a wheeled model (developed in [3]) to verify $\hat{\beta}$ for both wheeled mobile robots and human motion.

First, typical traction curves are generated (Fig. 3) for smooth, medium, and rough surfaces. (9) is validated by linearly increasing λ in a single wheel dynamic simulation. The resulting estimates of ω and $\dot{\omega}$ are used to determine α, using the slip velocity estimator in [4], and $\hat{\beta}$, using (9). shows the simulation results of the actual slope, β, compared to the estimated slope $\hat{\beta}$. Although the magnitudes do not coincide, they have the same sign and cross zero at the exact same time. In other words:

$$\begin{aligned} &\hat{\beta} > 0 \Rightarrow \beta > 0 \text{ (stable)} \\ &\hat{\beta} = 0 \Rightarrow \beta = 0 \text{ (marginally stable)} \\ &\hat{\beta} < 0 \Rightarrow \beta < 0 \text{ (unstable)} \end{aligned} \tag{10}$$

The critical comparison is whether both β and $\hat{\beta}$ cross zero simultaneously which indicates that either one can be used to indicate system stability. This simultaneous switching characteristic, between β and $\hat{\beta}$, are also observed while simulating more complicated time varying slip (including sinusoids or the addition of white noise). The increasing difference between β and $\hat{\beta}$ can be attributed to a greater amount of ground friction causing greater modeling uncertainly.

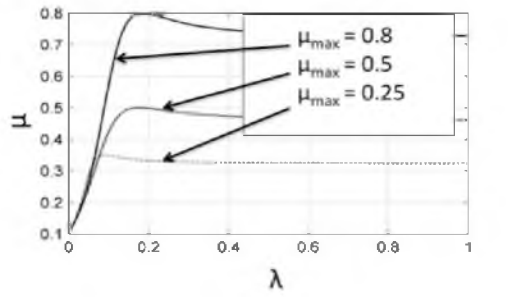

Fig. 3. Traction curves generated for validation.

Recall it is necessary to know the slope ($\hat{\beta} = \partial\tau / \partial\alpha$) opposed to *only* $\partial\tau(t)$ in order to identify the required $\pm\alpha$ modulation to approach the traction maximum.

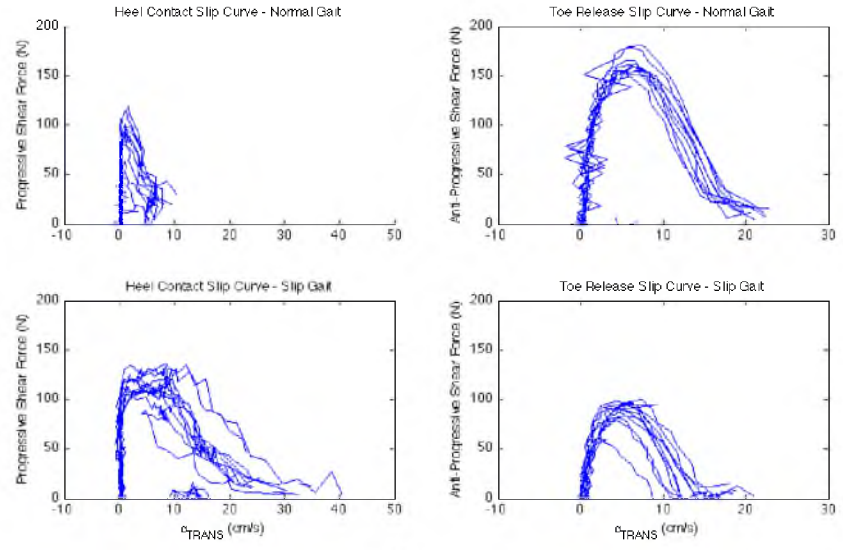

Fig. 2: α-τ slip curves generated for human slip. which correlate well to Fig. 1.

IV. Experimental Procedures

To experimentally verify $\hat{\beta}$, we used a motion analysis lab. The workspace of this lab, shown in the subfigures of Fig. 5, consisted of a passive-marker stereographic camera system to capture kinematic motion (primarily v_{TRANS}); and a three-axis force plate covered with a surface affording slip to capture traction forces. The

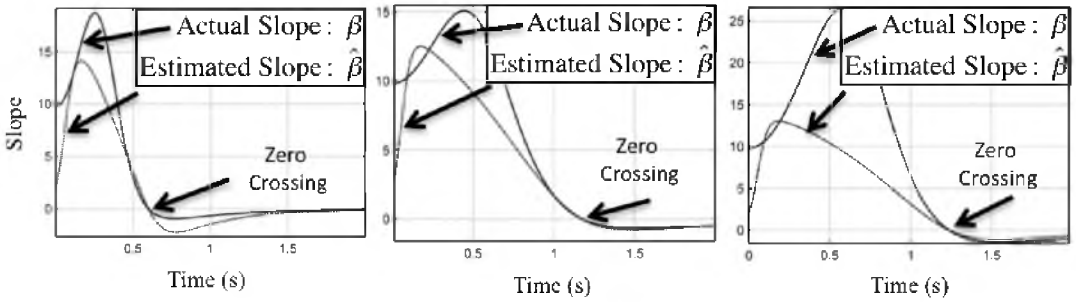

(a) $\mu_{\max} = 0.25$ (b) $\mu_{\max} = 0.50$ (c) $\mu_{\max} = 0.80$

Fig. 4. Traction curve slopes.

sampling frequencies, which are sufficient for capturing human motion (typically under 30 Hz), are 1000 Hz for both the kinematic motion capture cameras and the three-axis force plate. The slip surface consisted of a sheet of 'painter's plastic' secured to the floor surrounding the force plate and an additional loose sheet of plastic atop used to produce a shearing layer. Although experiments conducted in this paper use idealized velocity measurements, with a Vicon motion capture system, other avenues of our research have demonstrated that MEMS inertial sensors are capable of identifying the onset on slip [18].

The test gait of interest was a right foot slip and step-through, because it explored shear in both directions as well as a point where $\alpha_{TRANS} \rightarrow 0$. This procedure is illustrated in Fig. 5:

1. The subject approached the slip surface, and on heel strike begins to slip.
2. During slip, the subject continues his stride, causing his toes to contract the ground.
3. The subject regains balance by swinging his left foot forward, and in the process puts significantly more weight on the ball of his right (slipping) foot.
4. The subject removes his toes from ground.

V. Results

Fig. 6 shows the corresponding data for the procedure shown in Fig. 5. The left subfigures are the x and z positions, respectively. For this test, the zone between ~40-100 centiseconds is analyzed because this is the period in which the subject contacts the force plate. Fig. 7 presents an

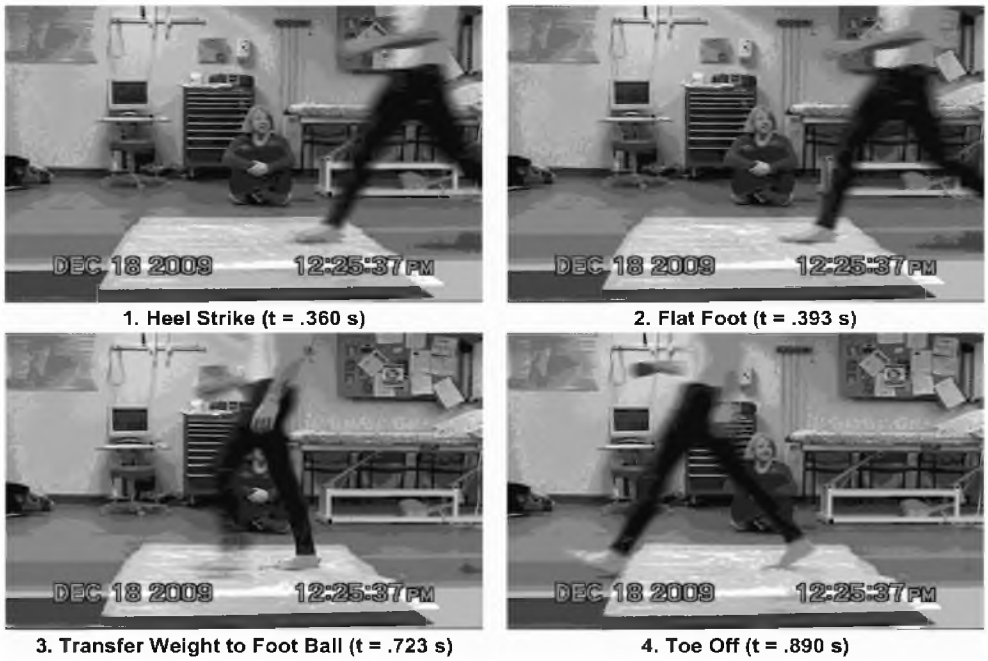

Fig. 5: Experimental Procedure. The walking subject steps on a 'slick surface' on top of a force plate with his right foot while a passive-marker stereographic camera system captures his motion. The corresponding data for this figure can is found in Fig. 6.

additional data set, using the same gait; although (instead of painter's plastic) glossy paper was used as the shearing layer. Both Fig. 6 and Fig. 7 are based on ankle velocity measurements. Fig. 8 is presented as a comparison using velocity of both ankle versus toe.

VI. Discussion and Future Work

All results show a good response to our predictions: Namely, $\hat{\beta}$ corresponds to traction force change. There are two discussion points of greatest interest: First, there must be a reasonable amount of slip to determine whether traction force is increasing or decreasing. Second, modeling and perhaps data fusion are critical for advancing this research.

Regarding the first discussion point, consider the heel contact (HC) and toe release (TR) regions of slip in Fig. 6 and Fig. 7 (HC: 32cs-53cs and 97cs-113cs, respectively; TR: 90cs-98cs and 113cs-117cs, respectively). These regions accurately predict our hypotheis of simultaneously changing signs of $\hat{\beta}$ and shear force. Notably, the relationship holds true for positive and negative axial shear, both of which exist in typical human gaits.

These common regions share high slip velocities. The other regions have low slip velocities and little correspondence between $\hat{\beta}$ and shear force as well as the occurrence of singularities. So, we hypothesize that as $\partial\alpha_{TRANS} \to 0$ reliability between $\hat{\beta}$ and shear force decreases.

The HC region has a larger period of correct correspondence between $\hat{\beta}$ and shear force than the TR region. We expect this is because Fig. 6 and Fig. 7 are developed from ankle velocities, which worked well for the HC region but not for the TR region. For the TR region, the heel begins to pick up and the foot deflects, relative to its ground contact at the toe, thus no longer providing an accurate representation of slip velocity. Additional data, seen in Fig. 8, supports this explanation as the correlation between $\hat{\beta}_{ankle}$ and shear force is better for the HC region, whereas the correlation between $\hat{\beta}_{toe}$ and shear force is better for the TR region.

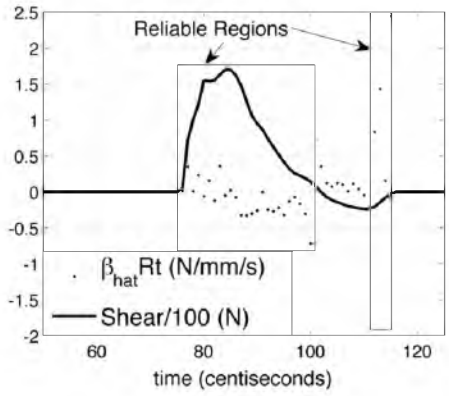

Fig. 7: Glossy paper slip data showing the difference between $\hat{\beta}$ and shear force.

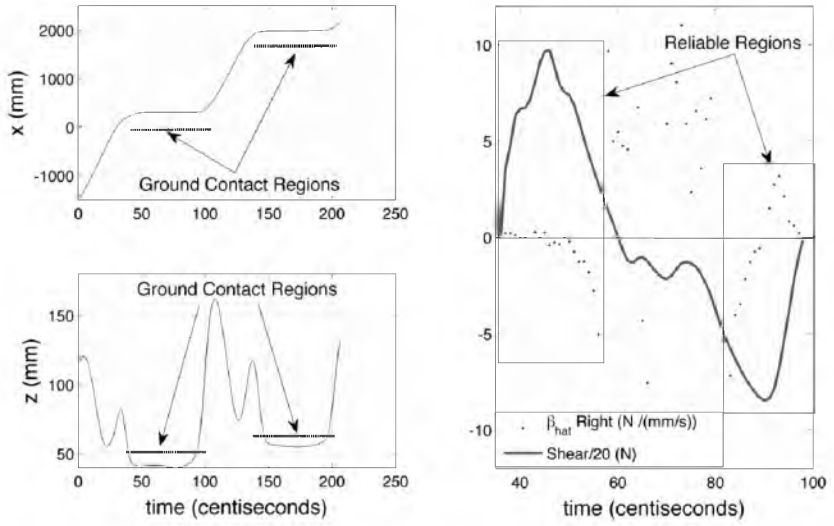

Fig. 6: Slip trial corresponding to Fig. 5. The left subfigures are the x and z ankle (only) positions, respectively; these are useful for knowing when the foot stops moving (x) and when it hits the ground (z). The period between ~40-100 centiseconds is in contact with the force plate. The right subfigure compares $\hat{\beta}$ to shear force.

Regarding further application of this research, modeling is critical in order to compute $\hat{\beta}$ online. A human dynamic model will be required to predict traction force in the absence of force plate readings. In addition, we discovered that the accuracy of beta depends where on the foot slip velocity is considered. In most cases, this is a point which is in contact with the ground. Our previously developed foot-bed sensors [19] are ideal for his purpose. Our future work will be in developing a dynamic gait model and wearable sensor arrangement capable of predicting traction force and accurately measuring slip velocity.

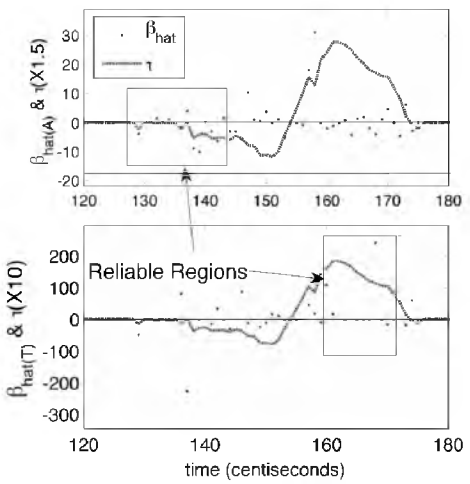

Fig. 8: Addition data comparing $\hat{\beta}$ to shear force for the ankle (top subfigure) and toe (bottom subfigure).

VII. Conclusion

This paper explored the analogs between wheel and human traction control principles. We developed a slip metric capable of identifying required actions to maximize traction force, based on the popular slip-traction curve and its slope. This research is an ideal proof of concept for future work involving wearable inertial measurement units, foot pressure sensors, and smart prosthetic design.

Acknowledgements

We would like to thank Bruce MacWilliams of Shiner's Childrens Hospital in Salt Lake City, Utah for access to motion capture facilities.

References

1. Norton, R., Campbell, J., Lee-Joe, T., Robinson, E. and Butler, M., *Circumstances of falls resulting in hip fractures among older people.* Journal of the American Geriatrics Society, 1997. 45(9): p. 5.
2. van der Burg, J. and P. Blazevic. *Anti-lock braking and traction control concept for all-terrain robotic vehicles.* in *Proceedings of the 1997 IEEE International Conference on Robotics and Automation, ICRA. Part 2 (of 4), Apr 20-25 1997.* 1997. Albuquerque, NM, USA: IEEE, Piscataway, NJ, USA.
3. Colli, V., G. Tomassi, and M. Scarano, *"Single Wheel" longitudinal traction control for electric vehicles.* IEEE Transactions on Power Electronics, 2006. 21(3): p. 799-808.
4. Terry, J.D. and M.A. Minor. *Traction estimation and control for mobile robots using the wheel slip velocity.* 2008. Piscataway, NJ, USA: IEEE.
5. Pacejka, H.B. and E. Bakker, *Magic formula tyre model,* in *Vehicle System Dynamics Proceedings of the 1st International Colloquium on Tyre Models of Vehicle Dynamics Analysis.* 1993, Swet. p. 1-18.
6. Fancher, P.S., Jr. and Z. Bareket, *Including roadway and tread factors in a semi-empirical model of truck tyres.* Vehicle System Dynamics, 1993. 21(SUPPL): p. 92-107.
7. Vechinski, C.R., C.E. Johnson, and R.L. Raper, *Evaluation of an empirical traction equation for forestry tires.* Journal of Terramechanics, 1998. 35(1): p. 55-67.
8. Shoop, S., et al., *Winter traction testing.* Automotive Engineering (Warrendale, Pennsylvania), 1994. 102(1): p. 75-78.
9. Sharp, R.S. and M. Bettella, *On the construction of a general numerical tyre shear force model from limited data.* Proceedings of the Institution of Mechanical Engineers, Part D: Journal of Automobile Engineering, 2003. 217(3): p. 165-172.
10. Gafvert, M. and J. Svendenius, *A novel semi-empirical tyre model for combined slips.* Vehicle System Dynamics, 2005. 43(5): p. 351-84.
11. Ortiz, A., et al., *Analysis and evaluation of a tyre model through test data obtained using the IMMa tyre test bench.* Vehicle System Dynamics, 2005. 43(SUPPL): p. 241-252.
12. Hughes, R.A., Comblath, D.R., *Guillain-Barre syndrome.* The Lancet, 2005. 336(9497): p. 1653-1666.
13. Chizeck, H.J., P.M. Selwan, and F.L. Merat. *A foot pressure sensor for use in lower extremity neuroprosthetic development.* 1985. Washington, DC, USA: Rehabilitation Eng. Soc. North America.
14. Smeesters, C., W.C. Hayes, and T.A. McMahon, *Disturbance type and gait speed affect fall direction and impact location.* Journal of Biomechanics, 2001. 34(3): p. 309-317.
15. Johansson, R. and M. Magnusson, *Human postural dynamics.* Crit Rev Biomed Eng, 1991. 18(6): p. 413-37.
16. van der Kooij, H., et al., *An adaptive model of sensory integration in a dynamic environment applied to human stance control.* Biol Cybern, 2001. 84(2): p. 103-15.
17. Cham, R. and M.S. Redfern, *Lower extremity corrective reactions to slip events.* Journal of Biomechanics, 2001. 34(11): p. 1439-45.
18. Lincoln, L., Bamberg, S.M., *Insole Sensor System for Real-Time Detection of Biped Slip*, in *2010 IEEE Engineering in Medicine and Biology Society.* 2010, IEEE: Buenos Aires, Argentina.
19. Bamberg, S., et al., *Gait analysis using a shoe-integrated wireless sensor system.* IEEE Transactions on Information Technology in Biomedicine, 2008. 12(4): p. 413-23.

The Potential to Fall Metric

The preceding paper identified significant problems with defining stability in bipeds. First, although the slip-traction curve of the foot-ground contact corresponds very to the wheel-ground contact, all this does is help define slipping stability of the biped's ground contact. In addition, the online metric for identifying slipping stability, $\hat{\beta}$, has low reliability, particularly when slip is near zero. This certainly is an issue with unreliable motions that do not involve much slip (such as tripping). Most importantly, this method of analysis does not describe or consider stability of the rest of the body.

The analysis for the preceding paper brought up the interesting point that bipeds, even in many resting postures, are inherently unstable. Therefore, stability is a poor metric to use in understanding movement of bipeds. It is more interesting, and informative, to identify *when* the biped loses its ability to balance and begins to fall. Potential to Fall (PF) was therefore proposed as a quantifiable metric associated with stability.

Potential to Fall of Bipeds Using Foot Kinematics

The following paper is reprinted with permission from Andrew Vogt, Andrew Merryweather, Kurt Beschorner, and Stacy Bamberg, *Potential to Fall of Bipeds Using Foot Kinematics*, 2013, 35$^{\text{th}}$ International Conference of the IEEE Engineering in Medicine and Biology Society (EMBC), July 2013.

At the time of publication, PF was simultaneously used as a qualitative description and a quantitative metric to analyze the probability of someone falling. After this publication (and as shown in the following chapters), the *likelihood of falling* is used as a qualitative descriptor, while *Potential to Fall* is used as a quantitative metric to measure the probability of someone falling.

Potential to Fall of Bipeds Using Foot Kinematics

Andrew Peter Vogt, Dr. Andrew Merryweather, Dr. Kurt Beschorner,
and Prof. Stacy J. M. Bamberg *IEEE Senior Member*

***Abstract*— This research compares normal to unexpected slipping gaits of healthy adults to detect potential to fall. Using various x, y, and z position analyses, including a Root Mean Squared Error (RMSE), significant differences are shown between normal and unexpected slipping gaits. Our results show that after heel strike of the slipping foot, the recovery foot rapidly changes position to restore balance and lower falling potential. We found RMSE of the recovery foot is significantly greater than the slipping foot, and that potential to fall is easily quantifiable through comparing normal to unexpected gaits. This research provides a solid foundations for a generalized understanding of fall potential for various gaits.**

I. INTRODUCTION

Liberty Mutual Research Institute for Safety had indicated nearly a 37% increase in same level falls experienced by people over the past 10 years. Falls on same level represent the second most costly form of disabling injury, representing $7.7 billion dollars per year [1], and are certainly an important issue for many researchers [2], [3], [4], [5], [6], [7] (to name a few).

A variety of attempts have been used to prevent falling. Our focus is to decrease the risk of fall through training. Studies show older adults are capable of reducing chances of falling by a factor of 7 if subjected to repeated slip events [8].

Movement Analysis (MA) is an excellent tool for improving physical skills by providing clear visual indicators of pathologic, in our case slipping, gait through comparison to a normal gait. These differences help define Potential to Fall (PF) and can be quantified using a Root Mean Squared Error (RMSE). Describing 'stability' of human motion is incredibly difficult and subjective; many could argue that even a walking gait is unstable motion. PF is developed in this paper as an alternative to stability applies to human motion. FP is shown to be high if a person has a higher probability of falling and low if otherwise.

This research continues an investigation of bipedal slip from two publications: [9] implemented a low cost wearable sensor capable of identifying slip in real time. [10] used a motion/force capture laboratory to evaluate force contact and slip relationships. Both publications only tested one or two subjects under predictable slipping conditions. Needing to direct the focus toward gait training, this paper looks at comparing kinematic data of multiple subjects experiencing an unexpected slip. The following sections outline out methods, results, a discussion of those results, future work, and conclusions.

A. P. Vogt is Faculty of Engineering at Salt Lake Community College, Salt Lake City, UT, U.S.A. andrew.peter.vogt@gmail.com
A. Merryweather is Faculty of Mechanical Engineering, University of Utah, Salt Lake City, UT, U.S.A. a.merryweather@utah.edu
K. Beschorner is Faculty of Materials Engineering, University of Wisconsin - Milwaukee, Wilwaukee, WI, U.S.A. beschorn@uwm.edu
S. J. M. Bamberg is Faculty of Mechanical Engineering, University of Utah, Salt Lake City, UT, U.S.A. phone: 801.585.9081 sjm.bamberg@utah.edu

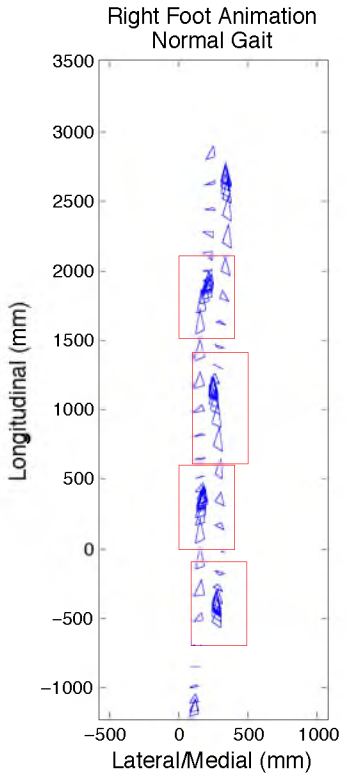

Fig. 1. Birdseye view of a typical normal gait. The four rectangles represent boundaries of the force plates. Valid subjects was selected if only one foot made contact with a unique force plate.

II. METHODS

Fig. 1 illustrates the testing environment. Four six-Degree of Freedom (DOF) Force Plates (FPs), illustrated with the red-outlined rectangles, were used with a right-left-right-left foot stepping pattern so that one foot would uniquely contact

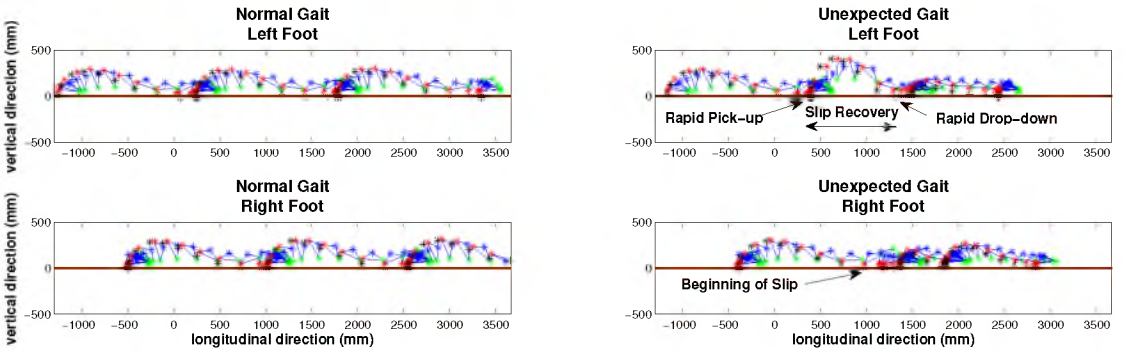

Fig. 2. Comparison of normal and unexpected slip walking gaits for both feet of Subject A, Trial 3. Red, blue, and green asterisk represent the heel, ankle, and toe markers, respectively. The black asterisk is a calculated heel marker which makes ground contact, and the brown line represents the ground.

one FP. With the exception of FP3, all FPs were always kept dry.

To ensure normal gait, and good baseline data, subjects were assured dry surface conditions during the first few trials. After the baseline trials, and without the subject's knowledge, a diluted glycerol solution, of 75% Glycerol and 25% Water, was applied to FP3. FPs 1, 2, and 4 were 400mm wide and 600mm long (see Fig. 1), and FP 3 was 400mm wide but 800mm long. FP3s extra length helped ensure force data was captured for both the normal and slipping event. It is difficult for subjects to see the difference in the size of FPs because the flooring surface on both FPs and the surrounding floor are the same size and color. Subjects are not told what the FPs are or their function, so they do not have a good reason to modify their gait to strike the FPs cleanly.

The data was collected as part of a larger project analyzing effects of aging and posture on slipping. Written informed consent was approved by the University of Wisconsin Internal Review Board. Subjects were fitted with 79 motion capture markers, a safety harness, and the same type of footwear.

Fig. 2 shows a sample comparison between normal and slip gaits for a single subject. The bold-brown solid line at zero represents ground, and the red, blue, and green markers represent the heel, ankle, and toe, respectively. For walking, the heel often strikes ground first. However, the heel markers do not coincide with the true heel contract point. A contact point, shown by the black marker on Fig. 2, is calculated using a known standing vertical distance each subject's heel marker and the ground. The left and right subfigures illustrate normal and unexpected slip gaits, respectively. The upper and lower subfigures show the left and right foot, respectively.

III. Analysis

Four subjects (A, B, C, and D), who experienced severe slips, were selected for analysis. Subject A had four recored normal gaits and Subjects B, C, and D had five recored normal gaits. Every subject had one unexpected slipping gait, where they were unaware of what trial the unexpected slip would occur. The results compared normal and unexpected three-dimensional kinematics, as shown in previous figures, and an RMSE calculation.

The RMSE compares each subjects's $n = 4$ or $n = 5$ normal gaits to each other, and to the unexpected slipping gait. Consider the following data sets:

$$K_{A,B,C,D} = \begin{bmatrix} k_{1,1} & \dots & k_{1,n} \\ \vdots & \vdots & \vdots \\ k_{300,1} & \dots & k_{300,n} \end{bmatrix} \tag{1}$$

$$U_{A,B,C,D} = \begin{bmatrix} u_1 \\ \vdots \\ k_{300} \end{bmatrix} \tag{2}$$

where K is an array of known data consisting of n normal gaits (number of rows) and 300 data points (number of columns) each. The set of unknown data, represented by U also has 300 data points, but only one trial dataset. There are 4 sets of unknown and known data sets corresponding to each of the 4 young and healthy subjects (A,B,C, and D). All data points in K and U are shifted to begin at a common x, y, and z coordinate. Data shifting ensure mores accurate averaging of the normal data, a clearer comparison between normal and unexpected data, and higher confidence that contact on FP3 happens at approximately the same time for all normal and unexpected trials. To ensure a clear correlation between the sets of normal data, an average is calculated,

$$K_{avg} = \begin{bmatrix} \frac{\sum_{i=1}^{n} k_{1,i}}{n} \\ \vdots \\ \frac{\sum_{i=1}^{n} k_{300,i}}{n} \end{bmatrix}. \tag{3}$$

Further insight comes from splitting the data at the point of heel contact for the unexpected trial of FP 3, resulting in

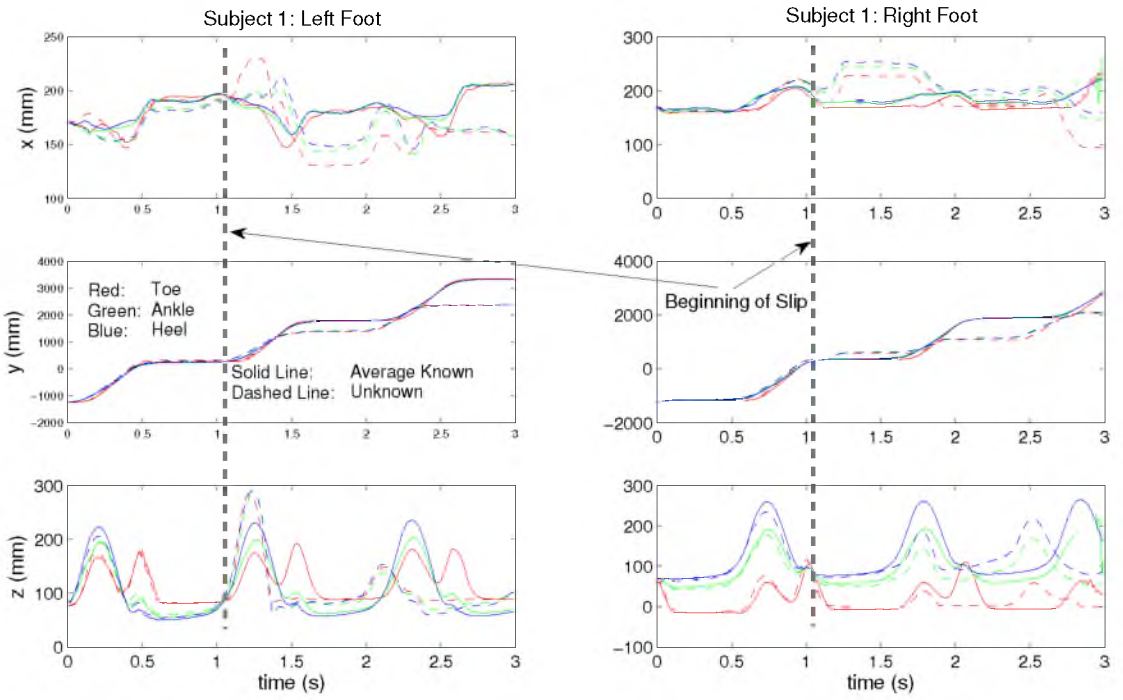

Fig. 3. Subject 1 x, y, and z markers for the toe, ankle, and heel. The solid line indicates the average normal trials and the dashed line indicates the unexpected trial. The vertical dashed line indicates the where unexpected slip occurs and the approximate time when the right foot strikes FP3.

split versions of (3)

$$K_{avg_{1\to FP3-1}} = \begin{bmatrix} kavg_1 \\ \vdots \\ kavg_{FP3-1} \end{bmatrix} \tag{4}$$

$$K_{avg_{FP3\to 300}} = \begin{bmatrix} kavg_{FP3} \\ \vdots \\ kavg_{300} \end{bmatrix} \tag{5}$$

In addition to visual inspection, RMSE is calculated to quantify the correlation between normal trials,

$$K_{RMSE_{1\to FP3-1}} = \frac{\sum_{i=1}^{FP3-1}}{FP3-1} \begin{bmatrix} \sqrt{(k_{avg_i} - k_{i,1})^2} \\ \vdots \\ \sqrt{(k_{avg_i} - k_{i,n})^2} \end{bmatrix}^T \tag{6}$$

$$K_{RMSE_{FP3\to 300}} = \frac{\sum_{i=FP3}^{300}}{300-(FP3-1)} \begin{bmatrix} \sqrt{(k_{avg_i} - k_{i,1})^2} \\ \vdots \\ \sqrt{(k_{avg_i} - k_{i,n})^2} \end{bmatrix}^T, \tag{7}$$

where (6,7) build row vectors compute the RMS value for each of the n trials. Then, the total RMSE for all n trials is computed using

$$\kappa_{RMSE_{1\to FP3-1}} = \frac{\sum_{j=1}^{n} K_{RMSE_{1\to FP3-1}}}{n} \tag{8}$$

$$\kappa_{RMSE_{FP3\to 300}} = \frac{\sum_{j=1}^{n} K_{RMSE_{FP3\to 300}}}{n} \tag{9}$$

where κ is the scalar sum of vector components of K_{RMSE}. One would expect $K_{RMSE_{1\to FP3-1}} < K_{RMSE_{FP3\to 300}}$ because gait naturally deviates over time.

While comparing similarities between known trials, RMSE also helps compare the differences between the average of the known trials to the unexpected trials. Similar to how (6) and (4) were split, the unexpected data is also split at the same point as follows

$$U_{1\to FP3-1} = \begin{bmatrix} u_1 \\ \vdots \\ u_{FP3-1} \end{bmatrix} \tag{10}$$

$$U_{FP3\to 300} = \begin{bmatrix} u_{FP3} \\ \vdots \\ u_{300} \end{bmatrix} \tag{11}$$

We also calculate the RMSE of both (10) and (11) datasets,

$$U_{RMSE_{1\rightarrow FP3-1}} = \frac{\sum_{i=1}^{FP3-1}}{FP3-1}|k_{avg_i} - u_i| \quad (12)$$

$$U_{RMSE_{FP3\rightarrow 300}} = \frac{\sum_{i=FP3}^{300}}{300-(FP3-1)}|k_{avg_i} - u_i|, \quad (13)$$

where (12,13) can be compared to (8,9) to correlate unknown and known datasets. A low numerical difference between (12) and (8) would indicate validity because the curves would be nearly coincident before slip. If a high numerical difference between (13) and (9) exists, then a significant PF would be expected.

IV. Results and Discussion

The kinematic results is shown in Fig. 2 and 3; the RMSE results are shown in Table I and Fig. 4.

A. Kinematics

When comparing normal to slip gaits, Fig. 2 illustrates a significant deviation between both the slipping (right) and recovery (left) feet. Normal gaits show a smooth transition as one foot strikes and the other gradually picks up to maintain balance. When a foot strikes a slippery surface, on the other hand, the other foot makes an abrupt motion to recover balance. Fig. 2 shows the left (recovery) foot lifts up and lets down in nearly half the longitudinal distance of a normal gait.

These rapid changes are also reflected in Fig. 3 which compare average normal (solid line) to unexpected slip (dashed line) for the toe (red), ankle (green), and heel (blue).The beginning of slip (thick gray dashed vertical) line, placed just after 1s, shows the approximate location of where the right foot strikes the FP3. Notice the rapid separation between the known (solid) and unknown (dashed) kinematics after unexpected slip. After this point, the normal gait is reasonably periodic, the unknown gait is quite stochastic. While slipping, the right foot instantaneously picks up speed in the medial and longitudinal directions with very little change in the vertical direction. After about 2s have passed, the unexpected gait begins to resume periodic behavior of a normal gait. The drastic difference between periodic illustrates that kinematics are an excellent metric for PF.

The left foot's recovery effort is shown by rapid vertical (z), and medial (x) motion. The vertical motion is no real surprise, and is already shown in Fig. 2, but the medial motion is quite interesting because it shows the effort to almost instantaneously widen the base of support to help prevent fall. The rapid medial motion of the toe, in relation to the other markers, further indicates this need to widen the base of support. These rapid movements indicates increased potential to fall. More subtle movements, are reflected as less potential to fall.

B. RMSE

RMSE data is presented Table I which combines all subject and foot marker data together with corresponding averages and standard deviations. Because of a potentially slippery FP3, the data is split between steps 1-2 and 3-4.

Fig. 4 presents the information in Table I graphically to better visualize PF of normal gaits, with respect to each other, and with respect to unexpected gaits.

Considering Table I, notice the rows of average known versus unexpected RMSE trials for steps 1-2. The RMSE average and standard deviation values are small and similar. When plotted, as the first subfigure in Fig. 4, the linear zero-intercept trend-lines have a nearly one-to-one slope. The indicates the first two steps of the unexpected trail can be classified as normal steps; if the subject anticipated a slip, it is likely this data would not be as well correlated. The one-to-one correlation helps conclude a low PF.

The one-to-one correlation supporting low PF is further supported when comparing rows of known versus unexpected RMSE for steps 3-4 on Table I and the second subfigure of Fig. 4. Between these steps, the known RMSE average and standard deviation values stay relatively low compared to the unexpected data; instead of a one-to-one correlation (for both mean and standard deviation), this now results in a 2.4-to-1 and 3.6-to-1 correlation for average and standard deviation, respectively. Both higher correlations indicated an elevated PF.

The previous comparison becomes stronger by comparing known RMSE trials of steps 1-2 and 3-4 presented by the third subfigure of Fig. 4. The slightly larger than one-to-one correlation is acceptable because gait naturally deviates over time; it is still far less than the unexpected gait presented in the second subfigure. PF is still low especially considering the longer time-lapse of the gait.

V. Future Work

PF analysis will be extended using more data from the subjects presented in this paper. We will look upper body markers to illustrate the center of mass movement in relation to the feet, and center of pressure, shear, and normal forces at the surface contact. All sources of data will be fused for an even clearer understanding of PF.

PF will help better understand bipedal movement in various gaits. Another upcoming project will instrument ski boots of skiers with Force Sensitive Resistors (FSRs) and Inertial Measurement Units (IMUs) to better understand their PF. The study in this paper is a critical foundation for understanding PF in skiers. Skiing instrumentation will be a great educational tool to help ski instructors better understand and control how students can reduce PF.

VI. Conclusion

Potential to fall (PF) is an important new metric because of the difficulty describing stability bipedal gaits. This paper showed various ways which kinematic foot maker data can

	Ankle						Toe						Heel						
Subject Average	Left (recovery)			Right (Slip)			Left (recovery)			Right (Slip)			Left (recovery)			Right (Slip)			
coordinates	x	y	z	x	y	z	x	y	z	x	y	z	x	y	z	x	y	z	
Avg. Known Trials	1.86	2.80	0.54	1.02	2.75	0.80	3.23	3.38	0.87	3.23	3.38	0.87	2.04	3.05	0.86	1.04	3.05	1.21	Steps 1-2
stdev +/-	0.87	1.17	0.12	0.60	1.86	0.46	1.94	0.81	0.06	1.94	0.81	0.06	1.11	0.88	0.25	0.59	1.89	0.68	
Unknown Trials	2.24	2.45	0.61	0.86	2.53	0.60	3.14	3.15	0.70	0.87	2.78	0.65	2.92	4.15	1.80	0.89	2.75	0.74	
stdev +/-	1.01	1.92	0.34	0.46	1.76	0.29	1.92	1.98	0.28	0.36	1.79	0.34	1.84	2.98	1.68	0.34	2.38	0.50	
Avg. Known Trials	2.85	5.70	0.90	2.85	4.88	1.56	3.70	6.03	1.06	3.95	6.03	1.06	2.90	5.63	1.41	2.80	5.05	1.41	Steps 2-4
stdev +/-	1.02	3.21	0.48	1.31	2.75	1.35	1.02	2.95	0.31	0.87	2.95	0.31	1.02	3.00	0.80	1.26	2.56	0.93	
Unknown Trials	4.83	13.55	2.43	3.80	14.38	2.80	7.38	15.25	2.68	3.19	16.33	1.78	4.93	15.53	4.08	3.25	14.90	3.93	
stdev +/-	3.24	14.76	0.79	0.60	1.86	0.46	4.39	15.12	0.93	1.94	11.93	0.53	3.30	14.22	1.34	0.73	11.49	1.54	

TABLE I

AVERAGE AND STANDARD DEVIATION FOR ANKLE, HEEL, AND TOE MARKER OF THE LEFT AND RIGHT FOOT VERSUS THE KNOWN AND UNKNOWN TRIALS OF THE FIRST AND LAST TWO STEPS. THIS AVERAGES AND STANDARD DEVIATIONS ON THE TABLE HELP INDICATE SIMILARITIES BETWEEN NORMAL GAITS AND DIFFERENCES BETWEEN THE NORMAL AND UNEXPECTED GAITS. UNITS ARE MM.

identify slip and PF. These kinematic foundations can effectively be applied to any biped with simple instrumentation, such as an IMU.

REFERENCES

[1] "Top 10 causes of disabling injuries 2007," tech. rep., 2010 Liberty Mutual Insurance Company, 2010.

[2] S. Gates, J. Fisher, M. Cooke, Y. Carter, and S. Lamb, "Multifactorial assessment and targeted intervention for preventing falls and injuries among older people in community and emergency care settings: systematic review and meta-analysis," *Bmj*, vol. 336, no. 7636, pp. 130–133, 2008.

[3] L. Gillespie, M. Robertson, W. Gillespie, S. Lamb, S. Gates, R. Cumming, and B. Rowe, "Interventions for preventing falls in older people living in the community," *Cochrane Database Syst Rev*, vol. 2, no. 2, 2009.

[4] T. Nikolaus and M. Bach, "Preventing falls in community-dwelling frail older people using a home intervention team (hit): results from the randomized falls-hit trial," *Journal of the American Geriatrics Society*, vol. 51, no. 3, pp. 300–305, 2003.

[5] M. Robertson, A. Campbell, M. Gardner, and N. Devlin, "Preventing injuries in older people by preventing falls: A meta-analysis of individual-level data," *Journal of the American geriatrics society*, vol. 50, no. 5, pp. 905–911, 2002.

[6] M. Tinetti, "Preventing falls in elderly persons," *New England journal of medicine*, vol. 348, no. 1, pp. 42–49, 2003.

[7] J. Zhang, K. Ishikawa-Takata, H. Yamazaki, T. Morita, and T. Ohta, "The effects of tai chi chuan on physiological function and fear of falling in the less robust elderly: an intervention study for preventing falls," *Archives of gerontology and geriatrics*, vol. 42, no. 2, pp. 107–116, 2006.

[8] Y. Pai, T. Bhatt, E. Wang, D. Espy, and M. Pavol, "Inoculation against falls: rapid adaptation by young and older adults to slips during daily activities," *Archives of physical medicine and rehabilitation*, vol. 91, no. 3, pp. 452–459, 2010.

[9] L. S. Lincoln and S. J. M. Bamberg, "Insole sensor system for real-time detection of biped slip," (Buenos Aires, Argentina), pp. 1449 – 1452, 2010. Biomimetic robotics;Bipedal gait;Bipedal locomotion;Detection rates;Human gait;Low costs;Numerous models;Real time;Real-time detection;Robot designers;Sensor systems;Traction control systems;Wearable sensor systems;.

[10] A. Vogt, L. Lincoln, S. J. M. Bamberg, and M. Minor, "Traction force characterization of human bipedal motion," in *IEEE/RSJ Intelligent RObots and Systems (IROS) Conference 2010. Taipei, Taiwan*, 2010.

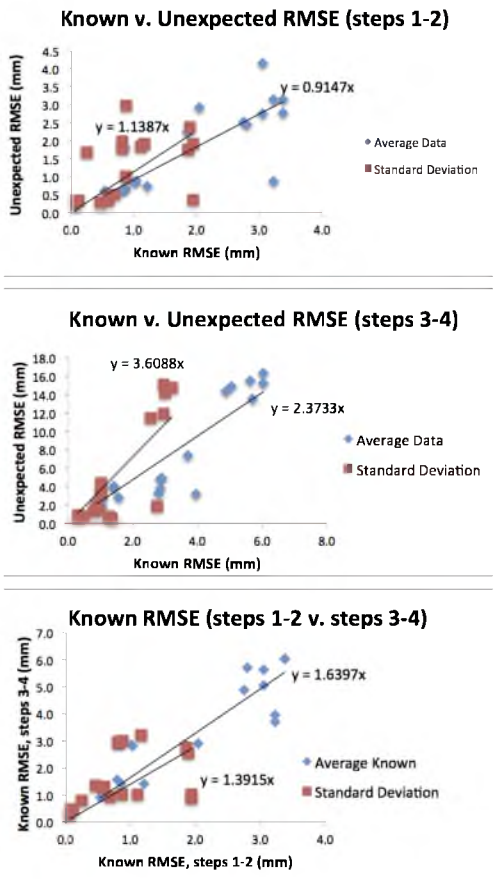

Fig. 4. Plots of RMSE and standard deviation with fitted trend lines having a y-intercept of zero. The trend-line help to correlate the potential of falling. The closer either the average or standard deviation trend-lines are to a slope of one (or one-to-one ratio) indicates a lot PF.

CHAPTER 3

USE OF KINEMATICS AND CENTER OF PRESSURE TO DETERMINE THE LIKELIHOOD OF FALLING AND DEVELOPMENT OF THE BIPEDAL POTENTIAL TO FALL METRIC

Chapter 2 established the motivation for and the fundamental basis of PF. It also begs important questions concerning the other factors that better help understand PF. This chapter looks at other important factors, namely upper body kinematics and foot center of pressure, to further develop a qualitative understanding of the likelihood of falling and quantitative PF metric. Both lead to a better understanding of upper body actions, which are critical to understanding falling. This chapter builds on the *Potential to Fall of Bipeds Using Foot Kinematics* EMBC 2013 conference paper to prepare for journal submission.

Introduction

Liberty Mutual Research Institute for Safety had indicated nearly a 37% increase in same-level falls experienced by people over the past 10 years. Falls on same level represent the second most costly form of disabling injury, representing $7.7 billion dollars per year [1], and fall prevention has therefore been a focus for many researchers.

Some of the best comparisons to are work are written by Xingda, Xinyao, *et al.* [2, 3]. Like our work, both of these publications look at fall and recovery efforts. Although [2] determined fall indicators using kinematics measures, it is not clear whether they have defined a metric, like Potential to Fall in our paper, to quantify the chance of fall. [3] illustrated the lower extremity response between successful recovery and falling after a slip. In contrast to this work, which looks at external force plate measurement and kinematic markers, [3] tracks muscular response. External

force measurements, in addition to kinematics, nicely extend this application to our novel noninvasive and inexpensive gait measurement tools.

One of the biggest focuses of this work is understanding recovery efforts after a slip has occurred. Lockhart *et al.* analyzed the effect of recovery from different age groups [4]. It found that older individuals have a much greater challenge when recovering from slip because their processes are much slower and less effective. However, Pai *et al.* studies show older adults are capable of reducing chances of falling by a factor of 7 if subjected to repeated slip events [5]. In addition to limbs first encountering a fall, this report discovers the importance of understanding how the human body recovers from fall.

In this chapter, kinematics and Center of Pressure (COP) were used as visual indicators of gait deviations between normal gait and an unexpected slip. These deviations were compared to qualitatively determine the likelihood of falling. Further understanding of the likelihood falling was supported with a quantitative PF metric based on Root Mean Squared Error (RMSE). While defining *stability* of human motion is inherently difficult and subjective, PF helps to objectify stability by comparing gait repeatability. In this analysis, it was found that periodic patterns were reflected in normal gaits, and also that they were also repeatable.

Unlike the EMBC 2013 conference publication, which focused only on foot kinematics, this chapter added hip and sternum kinematics and foot Center of Pressure (COP) to better understand interactions between the upper and lower body dynamics. These interactions indicated the of loss of balance which increased the probability of fall. In addition, numerical indicators of PF were identified.

Four young and healthy participants were selected from a larger study group because they experienced appreciable slip. This chapter compared the normal and unexpected slipping gait of these four subjects. The following sections describe methods, results, a discussion of those results, future work, and conclusions.

Methods

Fig. 3.1 presents a birds-eye view of the testing environment. Four 6-Degree of Freedom (DOF) Force Plates (FPs), illustrated with the red-outlined rectangles, were

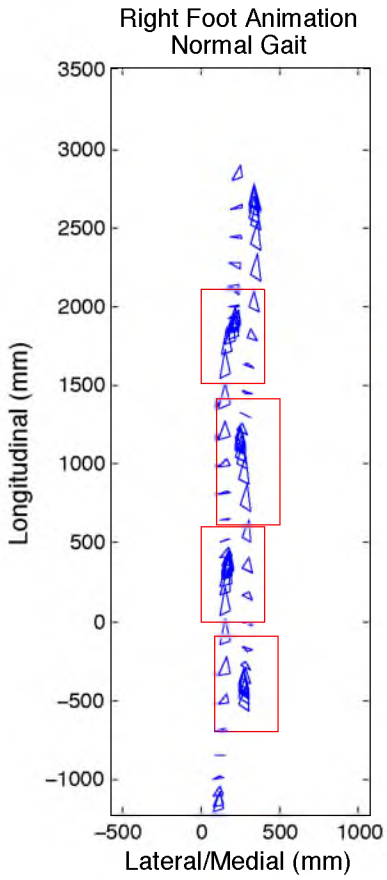

Figure 3.1: Birdseye view of a typical normal gait. The four rectangles represent boundaries of the force plates. Valid subjects were selected if only one foot made contact with a unique force plate.

used with a right-left-right-left foot stepping pattern so that one foot would uniquely contact one FP. With the exception of FP3, all FPs were always kept dry.

To capture normal gait for baseline data, subjects were told to expect dry surface conditions during the first few trials. After the baseline trials, and without the subject's knowledge, a diluted glycerol solution, of 90% Glycerol and 10% Water, was applied to FP3. FPs 1, 2, and 4 were 400mm wide and 600mm long (see Fig. 3.1), and FP 3 was 400mm wide but 800mm long. FP3s extra length helped ensure force data were captured for both the normal and slipping event. It was difficult for subjects to see the difference in the size of FPs because the flooring surface on both FPs and the surrounding floor were the same size and color. Subjects were not told

what the FPs are or their function, so they did not have a good reason to modify their gait to strike the FPs cleanly.

The data were collected as part of a larger project analyzing effects of aging and posture on slipping. Written informed consent was approved by the University of Wisconsin Internal Review Board. Subjects were fitted with 56 motion capture markers, a safety harness, and the same type of footwear.

Fig. 3.2 shows a sample comparison between selected foot markers of normal and slip gaits for a single subject. The bold-brown solid line at zero represents ground, and the red, blue, and green markers represent the heel, ankle, and toe, respectively. For walking, the heel often strikes ground first. However, the heel markers do not coincide with the true heel contract point. A contact point, shown by the black marker on Fig. 3.2, is calculated using a known standing vertical distance between each subject's heel marker and the ground. The left and right subfigures illustrate normal and unexpected slip gaits, respectively. The upper and lower subfigures show the left and right foot, respectively.

Analysis

Four subjects (A, B, C, and D) were selected from a larger study group because they experienced severe slips. Subject A had four recorded normal gaits and Subjects B, C, and D had five recorded normal gaits. Every subject had one unexpected

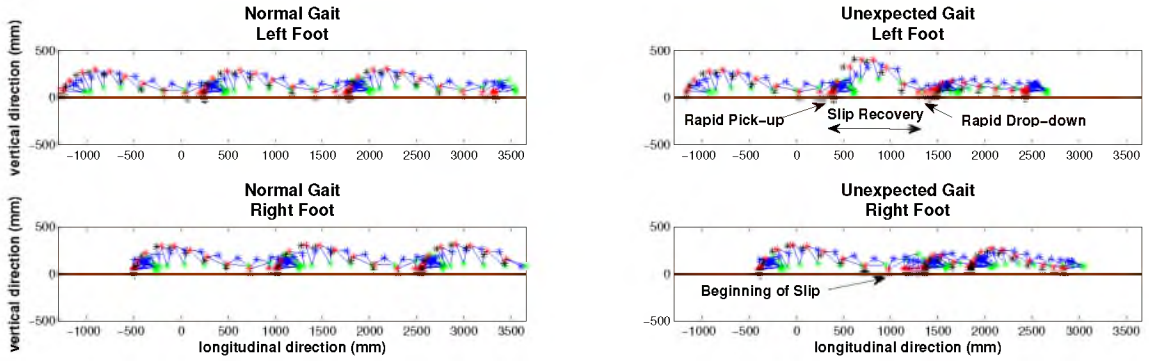

Figure 3.2: Comparison of normal and unexpected slip walking gaits for both feet of Subject A, Trial 3. Red, blue, and green asterisks represent the heel, ankle, and toe markers, respectively. The black asterisk is a calculated heel marker that makes ground contact, and the brown line represents the ground.

slipping gait, where they were unaware of what trial the unexpected slip would occur. The results compare the normal to unexpected (slipping) gait. Parameters compared include RMSE of kinematics, and analysis of COP. Changes in COP correspond to changes in posture and body position relative to the feet. By incorporating the relative upper and lower body kinematics with the COP analysis, an assessment can be made regarding the likelihood of falling by comparing motion of the upper body relative to the lower body.

Kinematic Data Processing

Consider the following data sets:

$$K_{A,B,C,D} = \begin{bmatrix} k_{1,1} & \dots & k_{1,n} \\ \vdots & \vdots & \vdots \\ k_{300,1} & \dots & k_{300,n} \end{bmatrix} \tag{3.1}$$

$$U_{A,B,C,D} = \begin{bmatrix} u_1 \\ \vdots \\ k_{300} \end{bmatrix} \tag{3.2}$$

where K is an array of known data consisting of n normal gaits (number of rows) and 300 data points (number of columns) each. $n = 4$ for subject A and $n = 5$ for subjects B, C, and D. The set of unknown data, represented by U, also has 300 data points, but only one trial dataset. There are 4 sets of unknown and known data sets corresponding to each of the 4 young and healthy subjects (A,B,C, and D). All data points in K and U are shifted to begin at a common x, y, and z coordinate. Data shifting ensures more accurate averaging of the normal data, a clearer comparison between normal and unexpected data, and higher confidence that contact on FP3 happens at approximately the same time for all normal and unexpected trials. To ensure a clear correlation between the sets of normal data, an average is calculated,

$$K_{avg} = \begin{bmatrix} \frac{\sum_{i=1}^{n} k_{1,i}}{n} \\ \vdots \\ \frac{\sum_{i=1}^{n} k_{300,i}}{n} \end{bmatrix}. \tag{3.3}$$

Root Mean Squared Error

The RMSE compares each subject's $n = 4$ or $n = 5$ normal gaits to each other, and to the unexpected slipping gait. Further insight comes from splitting the data at the point of heel contact for the unexpected trial of FP 3, resulting in two split versions of (3.3)

$$K_{avg_{1\to FP3-1}} = \begin{bmatrix} kavg_1 \\ \vdots \\ kavg_{FP3-1} \end{bmatrix} \tag{3.4}$$

$$K_{avg_{FP3\to 300}} = \begin{bmatrix} kavg_{FP3} \\ \vdots \\ kavg_{300} \end{bmatrix} \tag{3.5}$$

Visual inspection provides insight into the correlation of normal trials, and RMSE is calculated to quantify the correlation between normal trials,

$$K_{RMSE_{1\to FP3-1}} = \frac{\sum_{i=1}^{FP3-1}}{FP3-1} \begin{bmatrix} \sqrt{(k_{avg_i} - k_{i,1})^2} \\ \vdots \\ \sqrt{(k_{avg_i} - k_{i,n})^2} \end{bmatrix}^T \tag{3.6}$$

$$K_{RMSE_{FP3\to 300}} = \frac{\sum_{i=FP3}^{300}}{300-(FP3-1)} \begin{bmatrix} \sqrt{(k_{avg_i} - k_{i,1})^2} \\ \vdots \\ \sqrt{(k_{avg_i} - k_{i,n})^2} \end{bmatrix}^T, \tag{3.7}$$

where (3.6,3.7) build row vectors compute the RMS value for each of the n trials. Then, the total RMSE for all n trials is computed using

$$\kappa_{RMSE_{1\to FP3-1}} = \frac{\sum_{j=1}^{n} K_{RMSE_{1\to FP3-1}}}{n} \tag{3.8}$$

$$\kappa_{RMSE_{FP3\to 300}} = \frac{\sum_{j=1}^{n} K_{RMSE_{FP3\to 300}}}{n} \tag{3.9}$$

where κ is the scalar sum of vector components of K_{RMSE}. One would expect $K_{RMSE_{1\to FP3-1}} < K_{RMSE_{FP3\to 300}}$ because gait naturally deviates over time.

The RMSE is used to quantify each subject's changes in the unexpected trial as compared to the average known trails. Again, the unexpected trail is split at the time of heel strike,

$$U_{1\rightarrow FP3-1} = \begin{bmatrix} u_1 \\ \vdots \\ u_{FP3-1} \end{bmatrix} \tag{3.10}$$

$$U_{FP3\rightarrow 300} = \begin{bmatrix} u_{FP3} \\ \vdots \\ u_{300} \end{bmatrix} \tag{3.11}$$

RMSE of both (3.10) and (3.11) datasets is calculated,

$$U_{RMSE_{1\rightarrow FP3-1}} = \frac{\sum_{i=1}^{FP3-1}}{FP3-1}|k_{avg_i} - u_i| \tag{3.12}$$

$$U_{RMSE_{FP3\rightarrow 300}} = \frac{\sum_{i=FP3}^{300}}{300-(FP3-1)}|k_{avg_i} - u_i|, \tag{3.13}$$

where (3.12,3.13) can be compared to (3.8,3.9) to correlate unknown and known datasets. A low numerical difference between (3.12) and (3.8) would indicate a step without slip because the curves would be nearly coincident before slip. If a high numerical difference between (3.13) and (3.9) exists, then an unusual step would be indicated. This magnitude of this numerical difference represents repeatability between trials and is the foundation of the PF metric.

The Potential to Fall

Since the datasets are the same length, normal versus unknown slip RMSE values are plotted as the 'x' and 'y' values, respectively, on an x-y graph. If the data were perfectly repeatable, then all data points would fall on a line with a slope of one and a y-intercept of zero. Data with the lowest PF would also fall *on* this line. Data with increased PF would fall *off* this line. The PF metric is computed by fitting a linear trend line to the data and then determining deviation from a slope equal to one and a y-intercept equal to zero. PF encompasses two separate measures:

$$PF_1 = |trend_{slope} - 1| \tag{3.14}$$

$$PF_2 = |trend_{yInt}| \tag{3.15}$$

Where $trend_{slope}$ and $trend_{yInt}$ are the slope and y-intercepts of the trend line, respectively. Greater values from (3.14) or (3.15) indicate high PF.

Center of Pressure

All force plates were capable of obtaining translational force (referred to as a force) and rotational force (referred to as a moment) in the x, y, and z direction (the same directions as the kinematic x, y, and z). There was a malfunction with FP 4, so only FP 1, 2, and 3 were used in this analysis.

COP was calculated in the x (medial) and y (longitudinal) directions using the following equations:

$$COP_x = \frac{M_y}{F_z} \tag{3.16}$$

$$COP_y = \frac{M_x}{F_z} \tag{3.17}$$

M_y and M_x are the FP moment measured counter-clockwise about the y and x axes and F_z is the force in the z direction. The shear forces would only contribute to the COP calculation if the walking surface was significantly higher than the force plate surface. In this case, the walking surface was a think layer of vinyl (2-3 mm thickness), so the shear forces had minimal effect on (3.16) and (3.17).

Results and Discussion

The next two subsections discuss the likelihood of falling based on kinematics from the stereographic camera markers (Fig. 3.2, 3.3, and 3.4) and center of pressure from force plates (3.5, and 3.6). The last subsection discusses RMSE and the PF metric (Table 3.1 and Fig. 3.7).

Likelihood of Falling Using Kinematics

When comparing normal to slip gaits, Fig. 3.2 illustrates a significant deviation between both the slipping (right) and recovery (left) feet. Normal gaits smoothly transition as one foot strikes and the other gradually picks up to maintain balance. When one foot strikes a slippery surface, however, the other foot makes an abrupt motion to recover balance. Fig. 3.2 shows the left (recovery) foot lifts up and sets down in nearly half the longitudinal distance of a normal gait (see Slip Recovery arrow on the right top subfigure).

Fig. 3.3 and 3.4 compare average normal (solid line) to unexpected slip (dashed line) trials. While Fig. 3.3 compares the toe (red), ankle (green), heel (blue), and hips

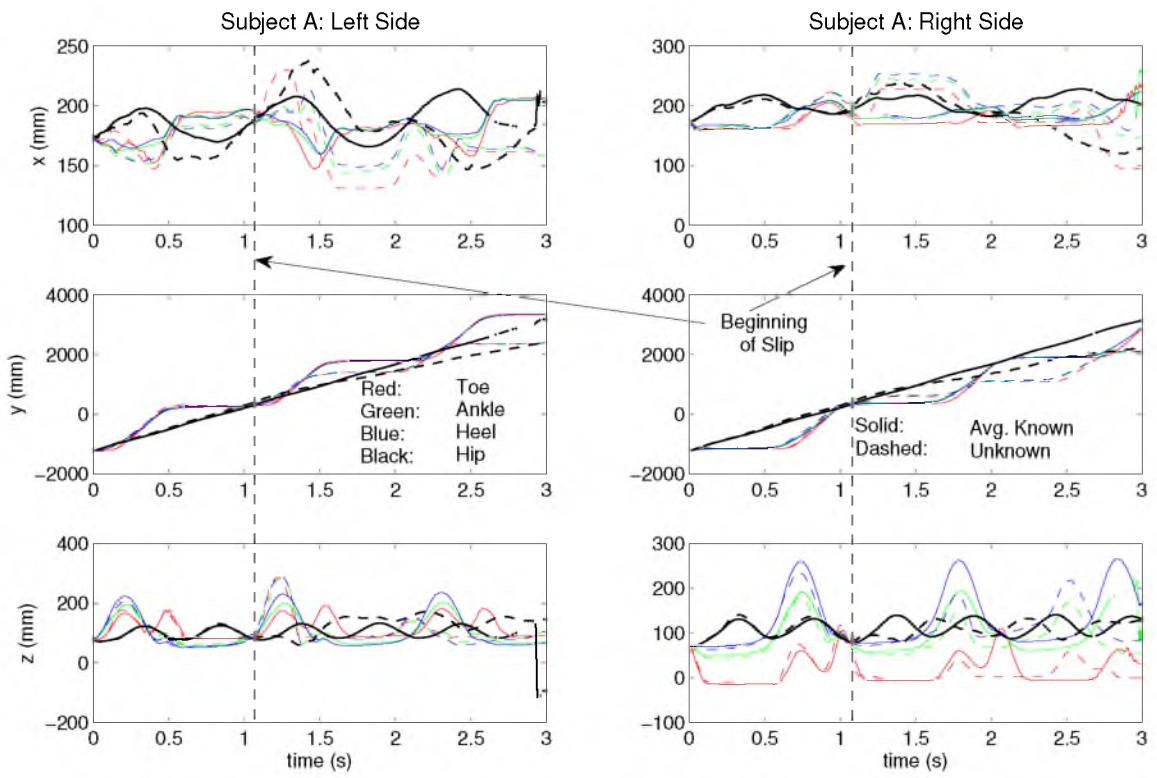

Figure 3.3: Subject 1 ankle and hip kinematic markers. The solid and dashed lines indicate the average normal unexpected trials, respectively. The vertical dashed line indicates when the unexpected slip occurred.

(thick black), Fig. 3.4 replaces the hip with the sternum. The hip and sternum are presented separately because otherwise, it would be difficult to tell them apart. The vertical dashed line indicates the time when the unexpected slip occurs. Before the vertical slip lines, the known (solid) and unknown (dashed) lines are nearly coincident. However, there is an obvious deviation after this point.

Before the beginning of slip, the known and unknown lines follow a very similar periodic behavior for all subjects. Differences following slip are most apparent with the hip and sternum, but minor changes are also apparent at the toe, ankle, and heel.

Understanding motions of the hip or sternum, caused by the initiation of slip, are important to suggesting the likelihood of falling. For example, if the upper body, shown by the motion of the hip or sternum, rapidly changes from smooth periodic motion, then it is likely the gait is not repeatable and unexpected motion can be inferred. This elevates the likelihood of falling because of unusual changes in position

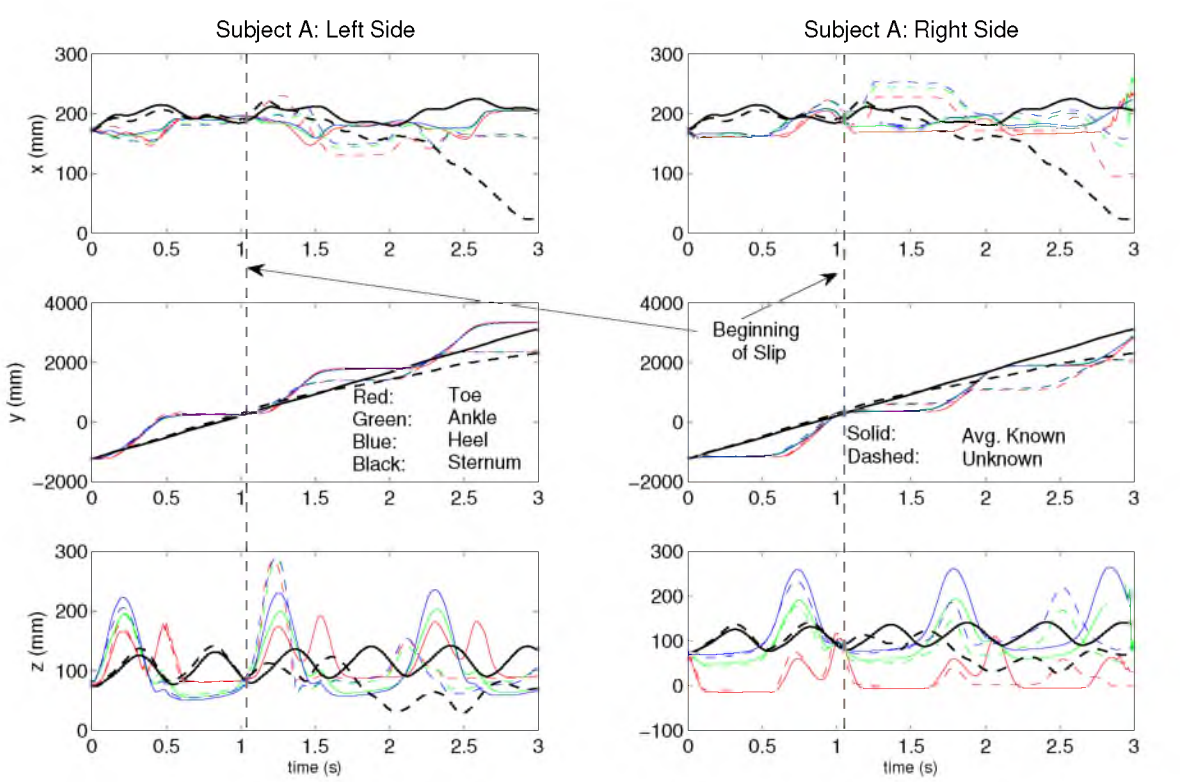

Figure 3.4: Subject 1 ankle and sternum kinematic markers. The solid and dashed lines indicate the average normal unexpected trials, respectively. The vertical dashed line indicates when the unexpected slip occurred.

of the upper body relative to the feet. The feet (toe, ankle, and heel) reflect similar changes in periodic behavior, which suggests that both the hips and feet are indicators of the likelihood of falling.

After about 2s have passed, the unexpected gait begins to resume periodic behavior of a normal gait. The recovery foot has a very rapid motion in the vertical (z) and medial (x) directions. The vertical motion is no real surprise, and is already shown in Fig. 3.2. Meanwhile, the sternum illustrates a large deviation and the medial motion of the foot and suggests an effort to widen the base of support to decrease the likelihood of falling for the upper body. The similarities of both slip and recovery suggest the foot as a viable candidate for the PF metric.

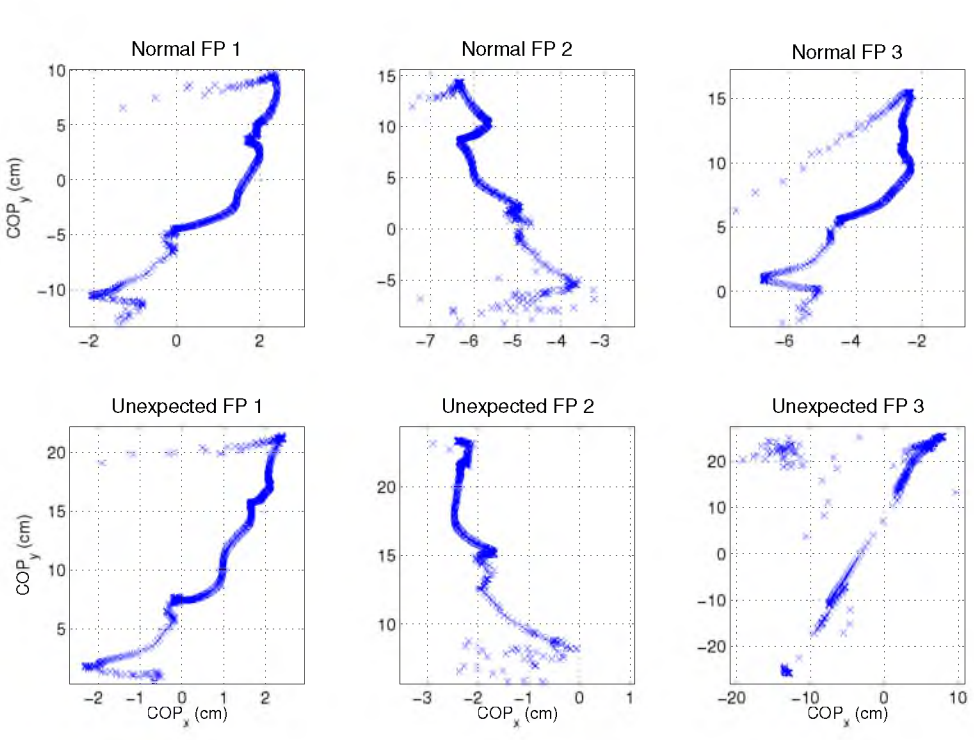

Figure 3.5: COP of Subject A comparing a normal to unexpected trials for FP 1, 2, and 3. Widely spread COP, in particular on FP 3, indicates a widened base of support, which is created when the likelihood of falling increases.

Likelihood of Falling Using Center of Pressure

In addition to the kinematics we have explored, up to this point, COP provides a unique understanding of the likelihood of falling. If the upper body is not cooperating with the lower body, then it is understandable that this will be reflected in the COP analysis.

For purposes of illustration, the x and y COP for a single trial of Subject A and Subject D are shown in Fig. 3.5 and 3.6, respectively. The trial selected for display is visually very similar to the others not shown in this paper. When using FPs, and the methods descried in (3.16) and (3.17), singularities are a common occurrence because most of the time throughout the experiment, the FPs are unloaded. Fig. 3.5 and 3.6 zoom into the portion that does not contain the singularities. The normal gait, shown in these figures, is very similar to [7]. The progression of COP presented in this book is an average value, which explains the jagged nature of these trials. However,

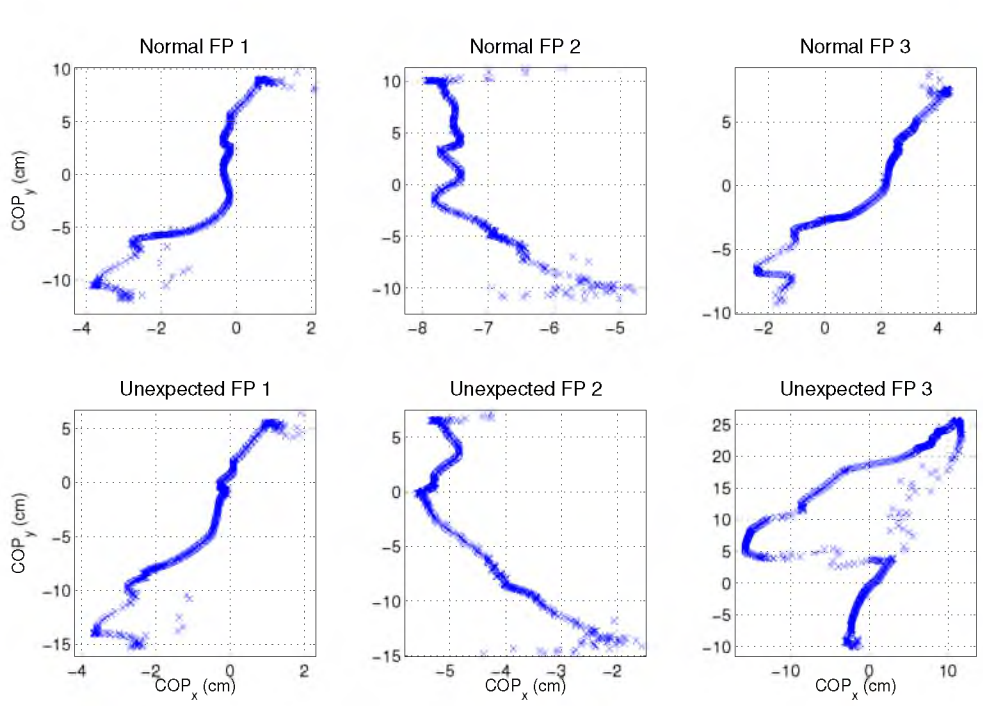

Figure 3.6: COP of Subject D comparing a normal to unexpected trials for FP 1, 2, and 3. Widely spread COP, in particular on FP 3, indicates a widened base of support, which is created when the likelihood of falling increases.

because there is only one unexpected slip trial, there is more insight to looking at one known trial versus the average of all the known trials.

Like the analysis of the upper body, the sternum in particular, versus the hip, we can see that the COP reflects the base of support. Again, this base of support is a clear indication of the likelihood of falling. Especially for the slipping foot, the COP spans a much wider range the the normal gait. Also, slip creates a discontinuity in COP on FP3, which helps add to this span. Although the recovery foot spans about the same amount of space as a normal gait, the trajectory of its COP is quite different. By looking closely, there is a greater density of COP markers toward the toes oppsed to the heel side of the FP.

Table 3.1: Average and Standard Deviation RMSE for ankle, heel, and toe marker of the left and right foot versus the normal and unexpected slipping trials of the first and last two steps. These are the scalar RMSE values given by (3.12) and (3.13). The averages and standard deviations on the table help indicate similarities between normal gaits and differences between the normal and unexpected gaits. Units are mm.

	Ankle						Toe						Heel						
Subject Average	**Left (recovery)**			**Right (Slip)**			**Left (recovery)**			**Right (Slip)**			**Left (recovery)**			**Right (Slip)**			
coordinates	x	y	z	x	y	z	x	y	z	x	y	z	x	y	z	x	y	z	
Avg. Normal Trials	1.9	2.8	0.5	1.0	2.8	0.8	3.2	3.4	0.9	3.2	3.4	0.9	2.0	3.1	0.9	1.0	3.1	1.2	**Steps 1-2**
stdev +/-	0.9	1.2	0.1	0.6	1.9	0.5	1.9	0.8	0.1	1.9	0.8	0.1	1.1	0.9	0.2	0.6	1.9	0.7	
Unknown Trials	2.2	2.5	0.6	0.9	2.5	0.6	3.1	3.1	0.7	0.9	2.8	0.7	2.9	4.2	1.8	0.9	2.8	0.7	
stdev +/-	1.0	1.9	0.3	0.5	1.8	0.3	1.9	2.0	0.3	0.4	1.8	0.3	1.8	3.0	1.7	0.3	2.4	0.5	
Avg. Normal Trials	2.9	5.7	0.9	2.9	4.9	1.6	3.7	6.0	1.1	4.0	6.0	1.1	2.9	5.6	1.4	2.8	5.1	1.4	**Steps 3-4**
stdev +/-	1.0	3.2	0.5	1.3	2.7	1.3	1.0	3.0	0.3	0.9	3.0	0.3	1.0	3.0	0.8	1.3	2.6	0.9	
Unknown Trials	4.8	13.6	2.4	3.8	14.4	2.8	7.4	15.3	2.7	3.2	16.3	1.8	4.9	15.5	4.1	3.3	14.9	3.9	
stdev +/-	3.2	14.8	0.8	0.6	1.9	0.5	4.4	15.1	0.9	1.9	11.9	0.5	3.3	14.2	1.3	0.7	11.5	1.5	

RMSE and the PF Metric

RMSE data are presented in Table 3.1, which combines all subject and foot marker data, together with corresponding averages and standard deviations. Because of a potentially slippery FP3, the data are split between steps 1-2 and 3-4.

Fig. 3.7 presents the average data in Table 3.1 graphically to better visualize PF of normal gaits, with respect to each other, and with respect to unexpected gaits. Because our prior work, [6], showed similar trends for average and standard deviation, only the average values are shown here. The dashed line has a slope of one and a y-intercept of zero. As priorly explained, the closer the data are to the dashed line, the lower the PF.

Considering Table 3.1, notice the rows of average normal versus unexpected slipping RMSE trials for steps 1-2. When plotted, as the first subfigure in Fig. 3.7, the linear trend-lines have slope close to one and a y-intercept close to zero. $PF_1 = 0.18$ and $PF_2 = 0.24$, displayed on the figure, are close to zero and so PF is low. If the subject anticipated a slip, it is likely these data would not be as well correlated.

Consider normal versus unexpected RMSE for steps 3-4 on Table 3.1 and the second subfigure of Fig. 3.7. Between these steps, the normal RMSE values stay relatively low compared to the unexpected data and the trend line is much further

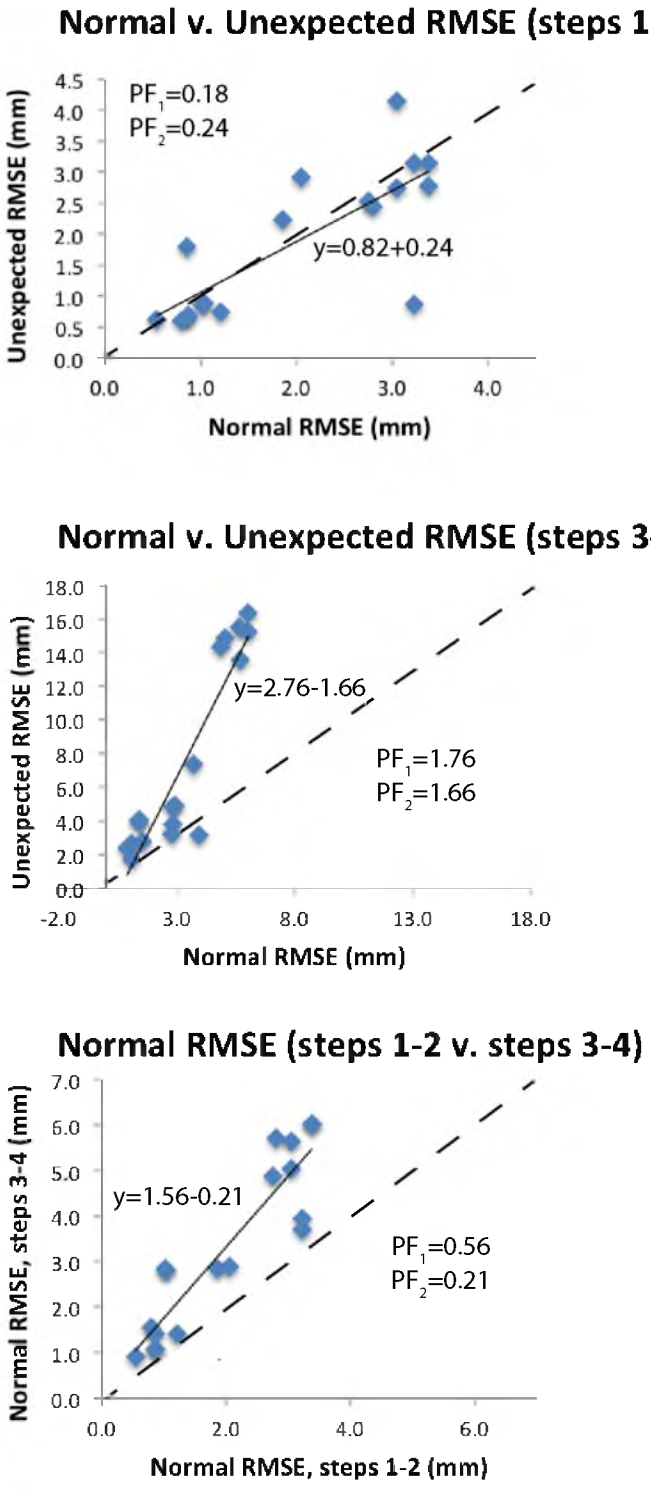

Figure 3.7: Plots of RMSE average with fitted trend lines compared to a slope of one with a y-intercept of zero (dashed line). Closer proximity of either of the data points of the trend lines to the dashed line implies less PF.

away from the dashed line. Compared to the first subfigure, $PF_1 = 1.76$ and $PF_2 = 1.66$ are significantly further from zero.

Comparing normal RMSE trials of steps 1-2 and 3-4, presented by the third subfigure of Fig. 3.7, helps to further support the low PF values in the first subfigure. While $PF_1 = 0.56$ is not as close to zero as the first subfigure, $PF_2 = 0.21$ is closer to zero. While this suggests total PF is not as low as the first subfigure, it is still low. However, because gait deviates over time, this result is expected.

Future and Other Work

PF helps to better understand bipedal movement in various gaits. Our biggest future goal with this work is to better understand the correlation between COP and the PF metric. But also, we are currently studying skiing PF, using instrumented insoles equipped with force sensitive resistors and inertial measurement units, to better understand PF in a generalized human gait. Understanding periodic motions, bases of support, the likelihood of falling, and the Potential to Fall metric have been particularly useful in this analysis. Skiing instrumentation has many applications, including a great educational tool for ski instructors to help novice, advanced, and even skiers with special needs.

Conclusion

Understanding the likelihood of falling is fundamental to describing stability of bipedal gaits. Using a quantifiable Potential to Fall (PF) metric further helped us to understand the likelihood of falling. This chapter applied kinematics from stereographic camera systems and the Center of Pressure (COP) from force plates to describe the likelihood of falling and quantify PF. These fundamental techniques can be applied to various types of bipedal locomotion, including scenarios where using laboratories for dynamic capture are unavailable.

References

[1] "Top 10 causes of disabling injuries 2007," 2010 Liberty Mutual Insurance Company, Tech. Rep., 2010.

[2] X. Hu and X. Qu, "Differentiating slip-induced falls from normal walking and successful recovery after slips using kinematic measures," *Ergonomics*, vol. 56, no. 5, pp. 856 – 867, 2013, accidental falls;Balance recoveries;Fall detection;falls;Normal walking;slips;Theoretical and experimental;. [Online]. Available: http://dx.doi.org/10.1080/00140139.2013.776705

[3] X. Qu, X. Hu, and F. L. Lew, "Differences in lower extremity muscular responses between successful and failed balance recovery after slips," *International Journal of Industrial Ergonomics*, vol. 42, no. 5, pp. 499 – 504, 2012, co-contraction;EMG;Fall prevention;Falls;Lower extremity;Medial gastrocnemius;Muscular activation;Peak amplitude;Rectus femoris;Slips;Tibialis anterior;. [Online]. Available: http://dx.doi.org/10.1016/j.ergon.2012.08.003

[4] T. E. Lockhart, J. L. Smith, and J. C. Woldstad, "Effects of aging on the biomechanics of slips and falls," *Human Factors*, vol. 47, no. 4, pp. 708 – 729, 2005, aging;Biomechanical parameters;Foot slips;Muscular strength;. [Online]. Available: http://dx.doi.org/10.1518/001872005775571014

[5] Y. Pai, T. Bhatt, E. Wang, D. Espy, and M. Pavol, "Inoculation against falls: rapid adaptation by young and older adults to slips during daily activities," *Archives of physical medicine and rehabilitation*, vol. 91, no. 3, pp. 452–459, 2010.

[6] A. Vogt, A. Merryweather, K. Beschorner, and S. J. M. Bamberg, "Potential to fall of bipeds using foot kinematics," in *International Conference of the IEEE Engineering in Medicine and Biology Society (EMBC) Conference 2013, Osaka, Japan*, 2013.

[7] J. Perry, *Gait Analysis*. Thorofare, NJ: SLACK Incorporated, 2010.

CHAPTER 4

USING A PILOT STUDY TO ESTABLISH EXPERIMENTAL METHODS FOR INEXPENSIVE INSTRUMENTED INSOLES USED IN DYNAMIC SKIING ANALYSIS

Certainly slip is not the only catalyst for increasing a persons PF. To investigate generalizability of PF to a broad spectrum of human locomotion, skiing was selected both because of its vast difference from walking and its inherent slip. The following content is to be published in an appropriate venue.

Introduction

Skiing equipment and ski theory is always changing. Professional ski instruction organizations, e.g., Professional Ski Instructors of America, frequently reorganize theories to better teach clients and other professionals. Properly supporting bodyweight allows efficient management of forces, primarily friction and normal forces, to control speed and direction. There are nearly infinite inverse kinematics (ways to move the body) to control ski forces. Maximizing efficiency, which to a large extent implies the skier has a low likelihood of falling, is a great challenge.

Skiing is relatively complex and has been described as a rhythm encompassing balance, finding support, and gliding [1]. Even for accomplished athletes, locomotion that effectively encompasses all these aspects takes years to refine. Quantified motion analysis helps to better understand the complexities of human locomotion. However, traditional motion capture laboratories cannot be used for skiing because they cannot effectively recreate the environment. Instead, wearable instrumentation can quantify motion in an established controlled mountain environment (e.g., a ski resort).

Wearable instrumentation has allowed skiing studies to drastically improve within the last few decades. Farrario *et al.* used a Fourier Analysis to predict trajectories of

skiers. They found trajectories of professional skiers, who take the same run under the same conditions, to have more repeatable results compared to casual skiers [2]. Coaches and scientists have instrumented skiers to get a better understanding of all of their intricate motions [3, 4, 5, 6, 7]. Some have used these tools to provide advanced feedback between students and coaches [3, 5, 6]. However, these systems are costly, prohibiting wide adaptation.

While using skiing as the method of locomotion, this work is primarily motivated toward better understanding the likelihood of falling during human locomotion. Comparing skiing studies to prior work on walking studies [8] provides a means to understand the likelihood of falling for generalized human locomotion. Unlike costly systems mentioned above, each insole can be fabricated for less than 200 U.S. dollars and could provide this valuable information to many skiers.

The remainder of this report covers Hardware and Software Development, the Original Experimental Methods, the Pilot Study, and Revised Experimental Methods (as a result of the Pilot Study).

Hardware and Software Development

The pilot study resulted in instrumented insoles to measure foot kinetics and kinematics. Other devices, such as skis or bindings, could have also been instrumented. However, the instrumented insoles had the advantage of being more transferrable to other skiers or ski equipment (a requirement of this study), they were inexpensive, and were protected from the elements. These insoles consisted of electronics that were placed in a cast, as shown in Fig. 4.1, and then embedded in blue silicone rubber, as shown in Fig. 4.2. Both left and right foot insoles, as shown in Fig. 4.2, were created and used in testing. Fig. 4.2 shows the original insoles where Vibrotactile Motors (VMs) were embedded in the insole. A later insole iteration, Fig. 4.1, tethered one VM outside the insole to be placed between the ski boot cuff and the skier's shin.

Contact dynamics were captured using 1.5 inch square force sensitive resistors (FSRs) (Interlink Electronics of Camarillo, California) toward the toe and heel of the foot and a 6-Degree Of Freedom (DOF) digital inertial measurement unit (IMU) (Sparkfun Electronics of Boulder, Colorado) placed in the center of the foot. The FSRs and IMU were fed into analog inputs of an Arduino Pro Mini Microcontroller

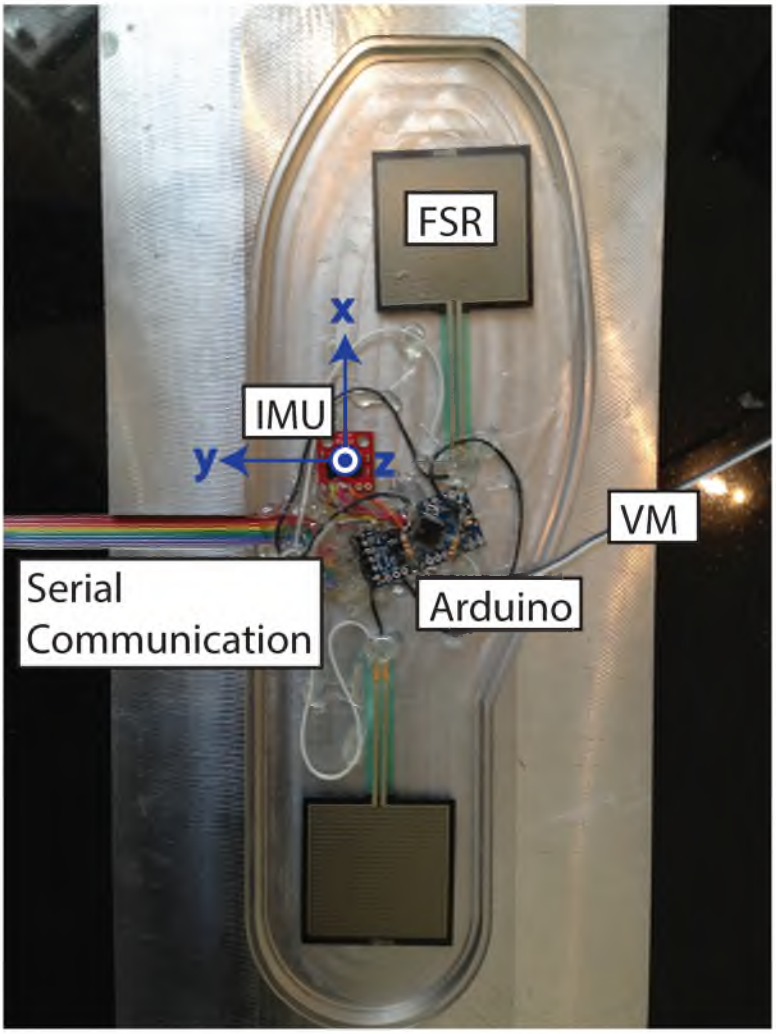

Figure 4.1: Photograph of equipment
used in instrumented insoles before pouring the mold. Unlike Fig. 4.2, where the Vibrotactile Motors (VMs) are embedded in the insole, this particular design tethers one VM out of the insole to be placed between the ski boot cuff and skier's shin.

(ATMEGA 328 3.3V 8 MHz Processor) (Dangi internet Electronics of Spain). Analog inputs of this Arduino read voltage in terms of bits; 0 to 1023 bits linearly correspond to an analog input of 0 to 3.3V. VM actuators were connected to the digital outputs on the Arduino.

Each FSR was connected in series with a 100Ω resistor, which provided an acceptable range of measurement for skiing. Placement of the FSR centroids were approximately 9 in apart to account for an average foot size and independently capture heel and toe kinetics.

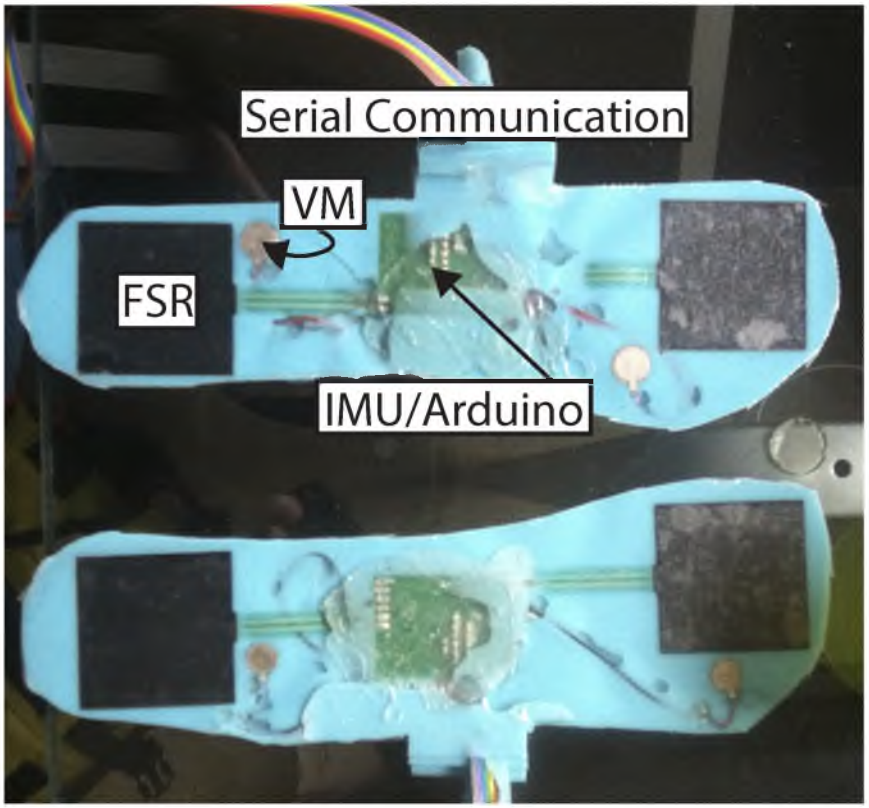

Figure 4.2: Photograph of instrumented insoles after pouring the mold. Unlike Fig. 4.1, a shield was used in the iteration to connect the electronics.

The FSRs and actuators were connected to the analog inputs and digital outputs, respectively, on the Arduino microcontroller. The analog input recorded in bits and the digital output produced either 0 or 3.3V. For calibration and testing, the Arduino was connected to the USB port of a laptop computer through a tether of approximately 18ft. Serial communication was used to transmit the data from the Arduino to the laptop at a 115200 baud rate. The FSRs were sampled at a rate of 155 Hz. The Arduino microcontroller was programmed using the Arduino programming environment. All data analysis was postprocessed using MATLAB.

Original Experimental Methods

The original proposal had the following specifications:

- Tests would be conducted on clear days with temperatures between 15 and 25 °F.

- The course would be controlled to be the same slope every time. This was set to be the run on the Chickadee green (beginner) slope at Snowbird Ski and Summer Resort (who provided written approval for the study) with six cones to define the testing course.

- Skiers would first take three runs within the cones as directed without any feedback. They would then do six runs with vibrotactile feedback, which would be randomized between three runs with a signal that is intended to appropriately cue the skier to shift weight between the left and right limbs, and three runs with a signal that has been constructed to provide random cues.

- Cones would be used to allow some control over both the course and the speed. A demonstration would be given first to indicate the appropriate speed.

Pilot Study

The pilot study was conducted with IRB approval (IRB 00055522) from the University of Utah.

Skiing Mechanics and Potential to Fall

Originally, the skier would receive vibrotactile and visual feedback. The thought was that comparing the two would lead to important conclusions regarding PF. The first iteration of the insole, shown in Fig. 4.2, had two Vibrotactile Motors (VMs) in the insole: one near the toe and the other near the heel. Before the pilot study, the rear VM would actuate for one second, signaling the skier that the turning signal was coming; one second later, the front VM would actuate for one second; and finally, the process would repeat after 4 s (seconds) elapsed. The expert skier in the pilot study identified that the vibrations in the boot completely dampened the VM signals, even when skiing smoothy with carving locomotion.

Since use of the VMs was not feasible, a new approach was developed to compare basic styles of beginning and advanced skiing; specifically that *individual improvements in skiing mechanics result in decreased likelihood of falling.*

Ski structure helps to explain the mechanics of beginning and advanced skiing styles. The structure of a ski, shown in Fig. 4.3, consists of tips, tail, top-sheet,

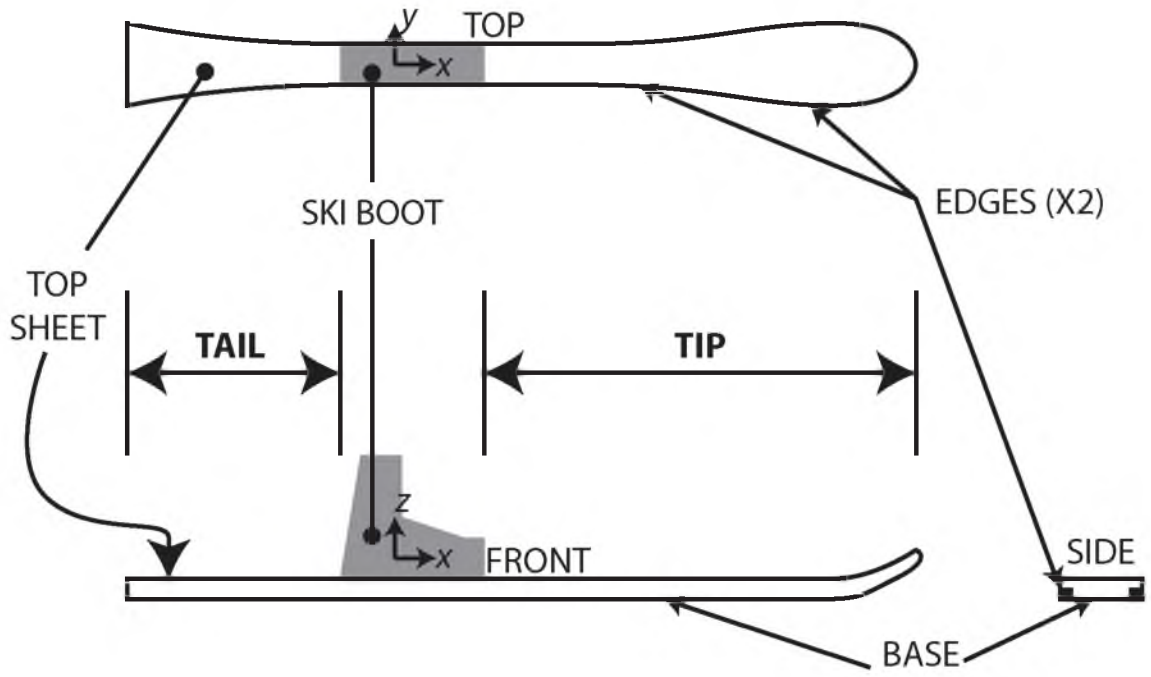

Figure 4.3: Structure of a typical ski. The ski boot is placed offset from the center toward the back, which causes the tip length to be longer than the tail.

base, and edges. Under normal skiing, the tip leads and the tail follows. The top sheet provides the primary structure (i.e., stiffness and vibration damping) of the ski, the base provides a low-friction surface to allow sliding with contacted snow, and the edges (on both sides) provide a medium to initiate turning and stopping of the ski. The inside and outside edges refer to the two edges closest and furthest to each other, respectively (i.e., the right edge of the left ski and the left edge of the right ski are the inside edges).

In order to maintain speed control, a skier will select an appropriate style based on weather, obstacles, ability, and fall line. Weather can include such factors as temperature, humidity, precipitation, and wind direction; and obstacles can include trees, rocks, other skiers, and varying snow conditions. Ability describes a skier's skill level and experience. Fall line, illustrated in Fig. 4.4, refers to the direction with the largest gradient in slope; in other words, the direction a ball would roll if placed on the ground.

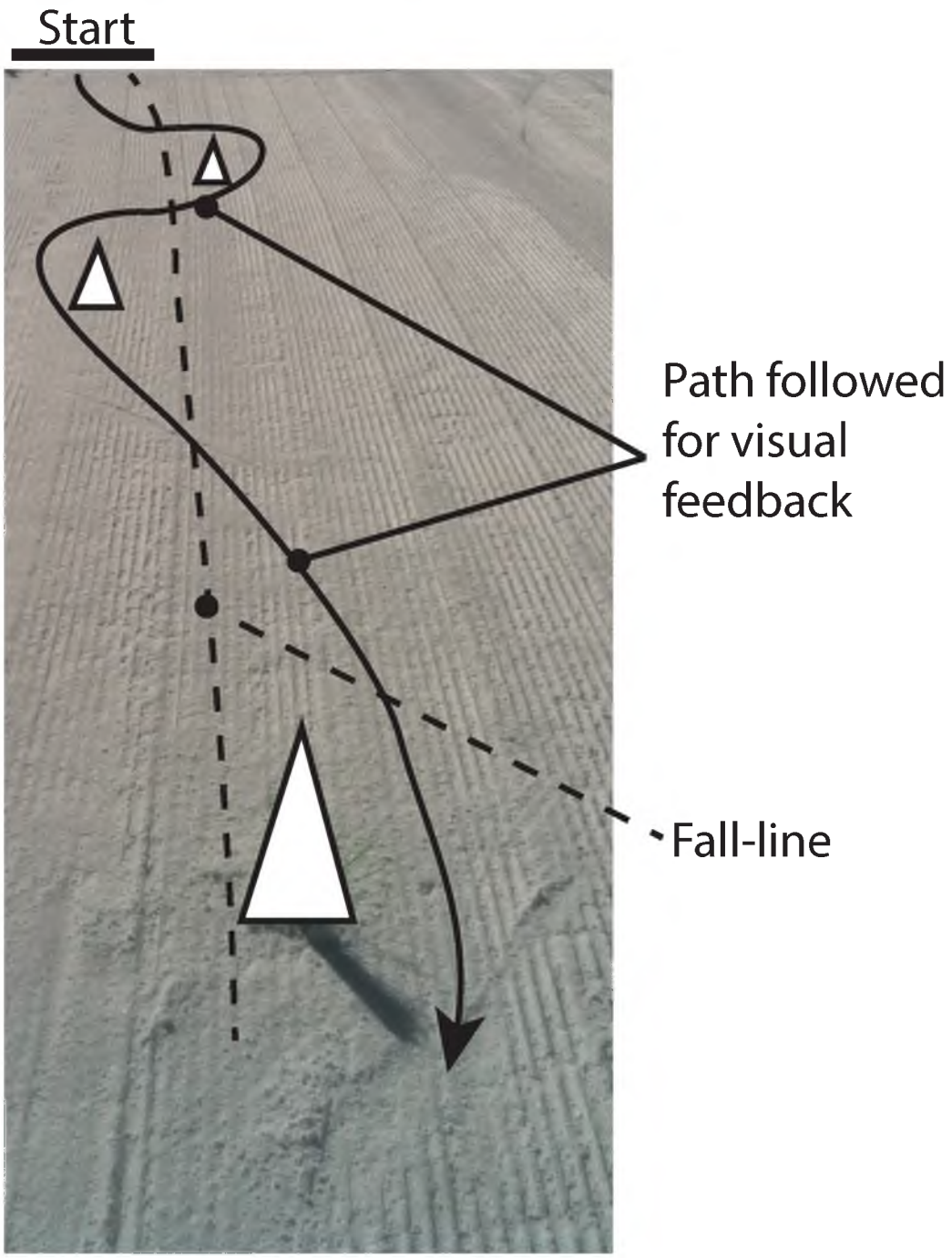

Figure 4.4: Path established from testing.
This path shows the first three turns. The white triangular markers represent where turning cones were placed. The turning markers help maintain speed control by ensuring the subject crosses the fall-line multiple times.

This study looks at two of the most fundamental skiing styles, as shown in Fig. 4.5: wedge style (WS) and parallel style (PS). The primary difference is that WS provides a greater resistance to motion of forward skier motion and is thus easier to control. As shown in Fig. 4.5, in WS, the ski tips have closer proximity than the tails.

The greater resistance to motion in WS is primarily due to the constraints from the skier's body. As the skier pushes the feet out to create a wedge shape, both the inside edge angles and resisting surface increase. Even when turning, the inside edges are engaged, maintaining more resistance to motion. Although edge angle from PS

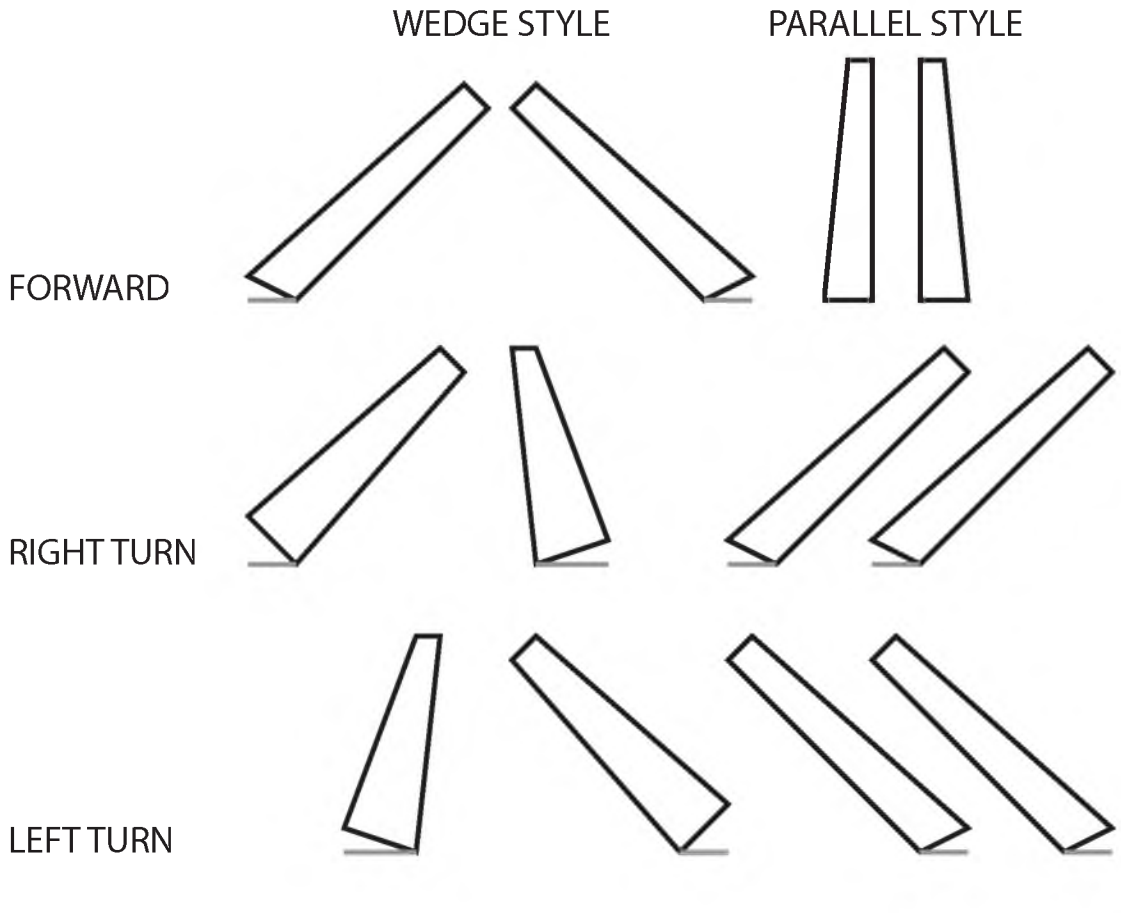

Figure 4.5: WS and PS illustrations of both skis traveling straight, right, and left. The small gray line at the bottom indicates whether the inside or outside edges are engaged. PS edging is significantly different than WS and is more difficult for subjects to control.

can be high, the use of one inside and one outside edge results in much less resistance to motion.

In addition, WS generally provides a much larger base of support due to a wider distribution of the skis across on the snow. In addition to easier speed control, the wedge more effectively resists moments caused by imbalance. This combination helps refine the above hypothesis such that *the mechanics of WS will yield a lower likelihood of falling than PS.*

Course Selection

The course was selected to ensure safety of skiers and enable consistent results. Fig. 4.4 illustrates the first few turning markers of the course, all of which follow the fall line. The course had a slope of 6 degrees, and the markers were spaced 11m apart parallel to the fall-line and 2m apart perpendicular to the fall line. As illustrated in Fig. 4.4, the subject skied around the outside of all the turning markers. The temperature was 22°F when the study was conducted (which was within the allowed 15-25 °F).

Pilot Study Results

Sample WS, Fig. 4.6, and PS, Fig. 4.7, plots display data gathered from the FSRs. On both plots, the first subfigure shows the actual forces recorded from the front and rear FSR, and the second subfigure shows the calculated Center of Pressure (COP). The reference point of the COP is the center of the heel. When using prior work to identify the likelihood of falling in walking studies, [8] illustrated that low likelihood of falling correlates with periodic motion. With the exception of the first 10 s (where the skier was ramping up speed) WS for both raw FSR and COP illustrates more periodic behavior than PS. Based on prior work, [8], which qualitatively indicated that periodic behavior led to lowered likelihood of falling, this again helps to refine the above hypothesis that *WS will yield a lower likelihood of falling than PS.*

Revised Experimental Methods

Following the pilot study, a few important changes were made to the original experimental methods to ensure the study could be completed.

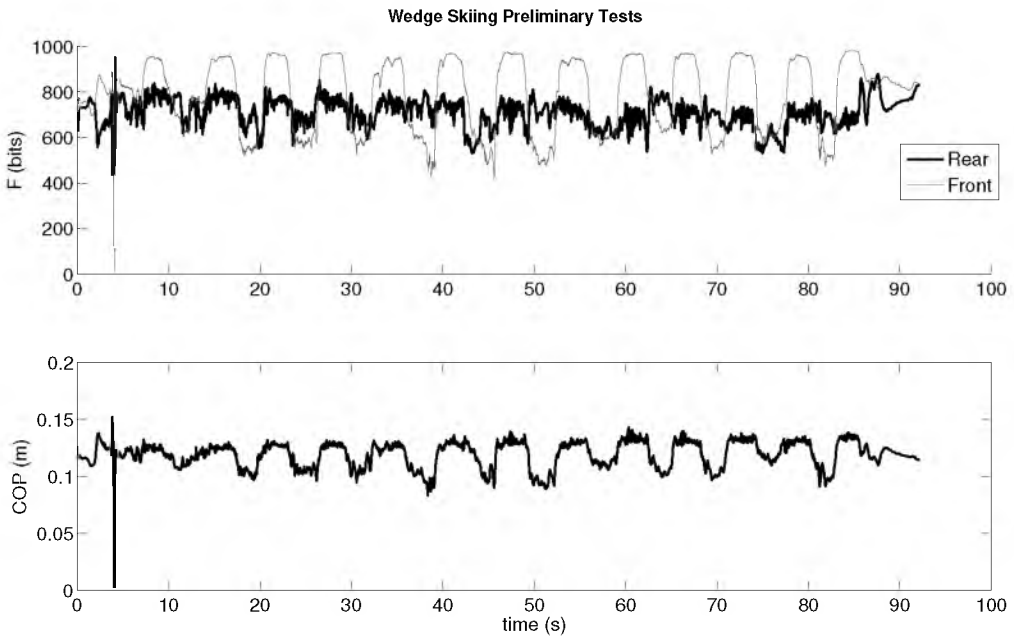

Figure 4.6: Preliminary Wedge Test. The top subfigure illustrates date from the front and rear FSRs. The FSRs had not been modeled for the preliminary tests, so they are expressed in bits directly received by the Arduino microcontroller. FSR modeling was done in the main study as shown in the next chapter. The bottom subfigure shows the COP as calculated from the front and rear FSRs.

- Due to lack of sensation, the toe VM was moved out of the insole and tethered so it could be placed between the shin and ski boot cuff. The VMs were still found to be ineffective and their use was discontinued.

- Subject recruitment goal: 12 subjects total, with approximately half being advanced or expert and half being novice or intermediate.

- Air temperature: Recorded for all subjects. Temperatures up to 65^{o}F due to spring testing conditions.

- 1 Baseline test where is the skier is instructed to ski how they are accustomed (no feedback whatsoever).

- 2 WS and 2 PS (4 total) tests where the skier will ski around the outside of the cones, used as visual feedback, as illustrated in the course presented in Fig. 4.4

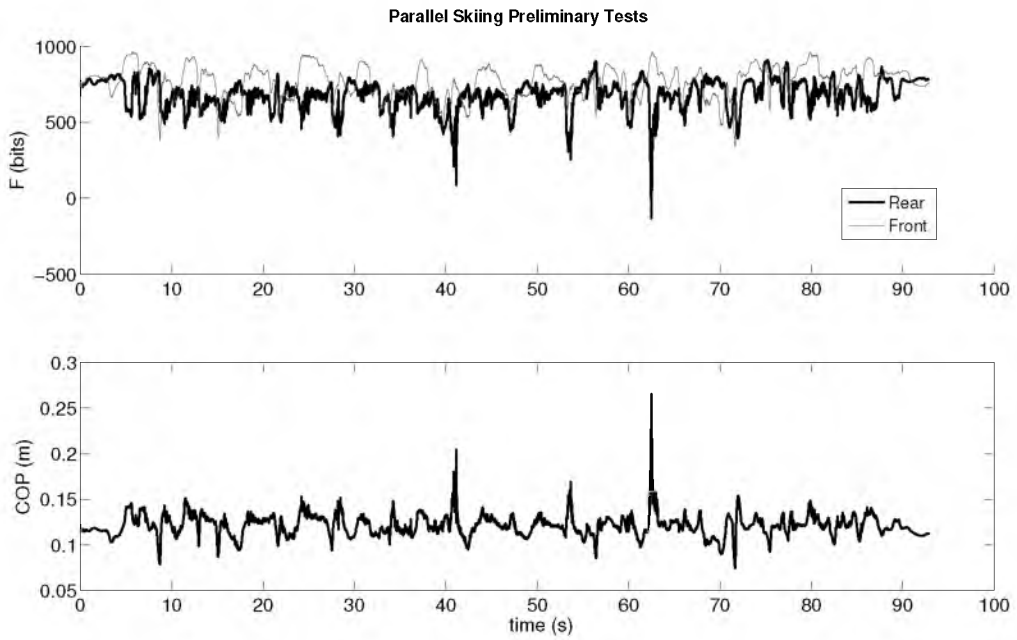

Figure

4.7: Preliminary Parallel Test. The top subfigure illustrates data from the front and rear FSRs. The FSRs had not been modeled for the preliminary tests, so they are expressed in bits directly received by the Arduino microcontroller. FSR modeling was done in the main study as shown in the next chapter. The bottom subfigure shows the COP as calculated from the front and rear FSRs. The COP for PS appears significantly more stochastic than WS, suggesting a higher likelihood of falling.

- Randomization of WS and PS ameliorated training effects.

Conclusion

This article establishes appropriate experimental methods for using instrumented insoles, with the primary intent of determining the likelihood of falling in skiers. The methods outlined in this article have been extended to a multiple-subject study. Further work on a multiple subject test is to be presented in a separate publication.

References

[1] S. Loland, "Alpine skiing technique: practical knowledge and scientific analysis," *Science and Skiing IV*, pp. 43–58, 2009.

[2] V. Ferrario, C. Sforza, G. Michielon, S. Dugnani, and F. Mauro, "A mathematical method for the analysis of trajectories in giant slalom," *Science and skiing*, pp. 107–115, 1997.

[3] F. Michahelles and B. Schiele, "Sensing and monitoring professional skiers," *Pervasive Computing, IEEE*, vol. 4, no. 3, pp. 40–45, 2005.

[4] T. Holleczek, C. Zysset, B. Arnrich, D. Roggen, and G. Troster, "Towards an interactive snowboarding assistance system," in *Wearable Computers, 2009. ISWC'09. International Symposium on.* IEEE, 2009, pp. 147–148.

[5] T. Holleczek, A. Regg, H. Harms, and G. Trster, "Textile pressure sensors for sports applications," in *Sensors, 2010 IEEE.* IEEE, 2010, pp. 732–737.

[6] P. Schaff, V. Senner, and F. Kaiser, "Pressure distribution measurements for the alpine skier–from the biomechanical high tech measurement to its application as swingbeep-feedback system," *Skiing and Science. London: E & FN Spon*, pp. 159–172, 1997.

[7] D. Tatsuno, T. Yoneyama, H. Kagawa, N. Scott, and K. Osada, "Measurement of ski deflection and ski–snow contacting pressure in an actual ski turn on the snow surface," *Science and skiing iV. Meyer & Meyer Sport (UK) Ltd, Maidenhead*, 2009.

[8] A. Vogt, A. Merryweather, K. Beschorner, and S. J. M. Bamberg, "Potential to fall of bipeds using foot kinematics," in *International Conference of the IEEE Engineering in Medicine and Biology Society (EMBC) Conference 2013, Osaka, Japan*, 2013.

CHAPTER 5

USE OF INSTRUMENTED INSOLES TO REFINE SKIING GAIT AND DETERMINE SKIING POTENTIAL TO FALL

Introduction

Modern skiing technique was first developed in the 1850s. Since then, the practice of skiing continues to be an involved science. Ski school and ski instruction organizations worldwide are continually trying to better understand ideal skiing movements. Even with advances in technology, the primary medium of feedback between ski instructors and students is based on visual observation (instructor of student, or student of instructor) and spoken feedback. This method is helpful, but it is inherently qualitative and provides few details about foot-boot interactions.

Biological instrumentation, or bioinstrumentiation, has been used by many researchers to better understand human motion both in a lab setting and out in the real world. Instrumented insoles have been used by our lab group to evaluate biomechanics of human motion [1, 2, 3, 4]. The primary advantage of these insoles are that they can be used in nontraditional laboratory settings. Effectively replicating a skiing environment is nearly impossible, so instrumented insoles provide a solution that can be used in the field. A pilot study, presented in the previous chapter, refined appropriate methods for using instrumented insoles adapted for ski boots. Using multiple subjects, the objective of this study is to use two types of skiers (intermediate versus expert) and two types of styles of skiing (wedge versus parallel) to understand the qualitative likelihood of falling, develop a quantitative Potential to Fall (PF) metric applied to skiing.

The following sections go into details on experimental methods, data analysis, results and discussion, future work, and conclusions.

Experimental Design

IRB Approval and Subject Demographics

This study was conducted with Internal Review Board (IRB) approval (IRB 00055522) from the University of Utah. 12 total subjects, 5 female and 7 male, were tested, with an age range of 20 to 60 years old. Test subjects were required to perform both Wedge Style (WS) and Parallel Style (PS) skiing. Interviews classified whether subjects were intermediate or expert skiers. A subject was classified as an expert if they had received extensive training, including ski instructing or ski racing. All other subjects were classified as intermediates. All the of expert subjects received training from the Professional Ski Instructors of America (PSIA).

All subjects were required to be able to perform WS and PS skiing. There were 4 expert skiers in this dataset (subjects 002, 003, 004, and 010). 2 were male and 2 were female and the average age was 50 years old. In addition to understanding changes

Figure 5.1: Example test subject,
followed by the researchers, undergoing visual feedback. The researcher followed with a laptop and collected data from the insoles. Courtesy of Powder Shots photography.

in the likelihood of falling from WS to PS skiing across all skiers, a secondary goal was to understand the likelihood of falling between intermediate and expert skiers.

Subject Testing Procedures

First, the basic procedures of the test were described to each subject, and then informed consent was performed. After putting on the ski boots with the insoles inside, a procedure was performed to calibrate the FSRs. The skiing tests included at least five parts, including baseline, wedge style, and parallel style skiing as described in the following sections. The majority of tests utilized a specified test course providing users visual feedback. As shown in Fig. 5.1, the researcher, holding a laptop computer, followed the test subject. Data from the test subject streamed to the laptop using a serial communication tether.

Hardware

The same equipment is used here as was in the pilot study. However, the IMU was used extensively in this study. The IMU (Digital Combo Board - 6-Degrees Of Freedom ITG3200/ADXL345 manufactured by Sparkfun Electronics of Boulder, Colorado) consists of a triaxial accelerometer and triaxial gyroscope. The IMU and the Arduino microcontroller used the I^2C communication protocol and was implemented by Johnson [5]. Because of concerns of vibration sensitivity, the IMU was placed in the center of the insole in the location of the arch to reduce forces on the circuitry. Further protection as well as vibration damping were provided by embedding the IMU into the blue silicone rubber insole material.

MicroElectricalMechanical Systems (MEMS) are used because they can be very small (under 1 mm^2), have high durability, and use little power [6, 7]. Accelerometers and gyroscopes have been used for many applications, including fall detection. Accelerometers measure translational acceleration and gyroscopes measure rotational speed. Chen attached accelerometers to the waist of individuals. He discovered that the magnitude of acceleration could be used to indicate if a fall occurred [8]. Bourke used a bi-axial gyroscope to differentiate between daily living activities and falls [9]. Bachlin used visual and auditory feedback from accelerometers to improve swimmer locomotion [10].

Calibration

The FSR calibration was performed before the subjects put on skis. If possible, the instrumented insoles were placed between the relatively rigid shell and liner of the boot to minimize FSR deformation, and to allow the IMU to maintain a constant orientation with respect to the boot. Subjects were instructed to elevate their feet, relax the muscles in their foot, and try to keep their foot as level to the ground as possible. The purpose was to provide a baseline reading of the sensors while unloaded. Data were collected for approximately 10 s, and then the average and standard deviation for the FSRs were calculated.

At the beginning of every test, subjects were asked to stand with their skis parallel before beginning the test. Understanding that they did not want to slide down the hill, the subjects would naturally position *both* skis perpendicular to the fall-line (the direction of steepest gradient). This started subjects in a safe position and provided data prior to movement. Data collected prior to movement were used for IMU calibration.

Baseline Testing

All tests were conducted on the same location on a slope of approximately 6 degrees. For the baseline test, subjects were instructed to ski down the slope and control speed by turning. The purpose was to collect data corresponding to the subject's baseline skiing abilities prior to instructions and feedback.

Wedge and Parallel Testing

The WS and PS test course consisted of 20 cones. Each cone was placed 11m down the fall-line and 2m across the fall-line from the prior cone. Subjects were instructed to turn around the outside (the furthest possible distance front the center of the course) of each of the cones. A minimum of two WS and two PS tests were conducted for each subject. This order was randomized before the test began.

Methods

FSR Unit Conversion

The primary details of the hardware and software development are described in the previous chapter. The FSRs were connected to analog inputs of the Arduino,

converted using an 8 bit ADC, and recorded as bits (with 0-1023 corresponding to 0-3.3V). Force was modeled by placing an FSR, cast in a silicone insole, into a compression testing machine, as shown in Fig. 5.2. Then, in increments of approximately 10 lb, the voltage, expressed in bits, was recorded from the voltage divider circuit attached to the Arduino. The actual data capture is illustrated in Fig. 5.3. To capture the nonlinear behavior and yet not damage the FSR with excessively large force, a maximum of 100 lb was applied from the compression test. The force recorded in the compression test was calibrated to the weight of the circular compression disc. The pressure, p, on both the compression disc and the FSR was equivalent. The

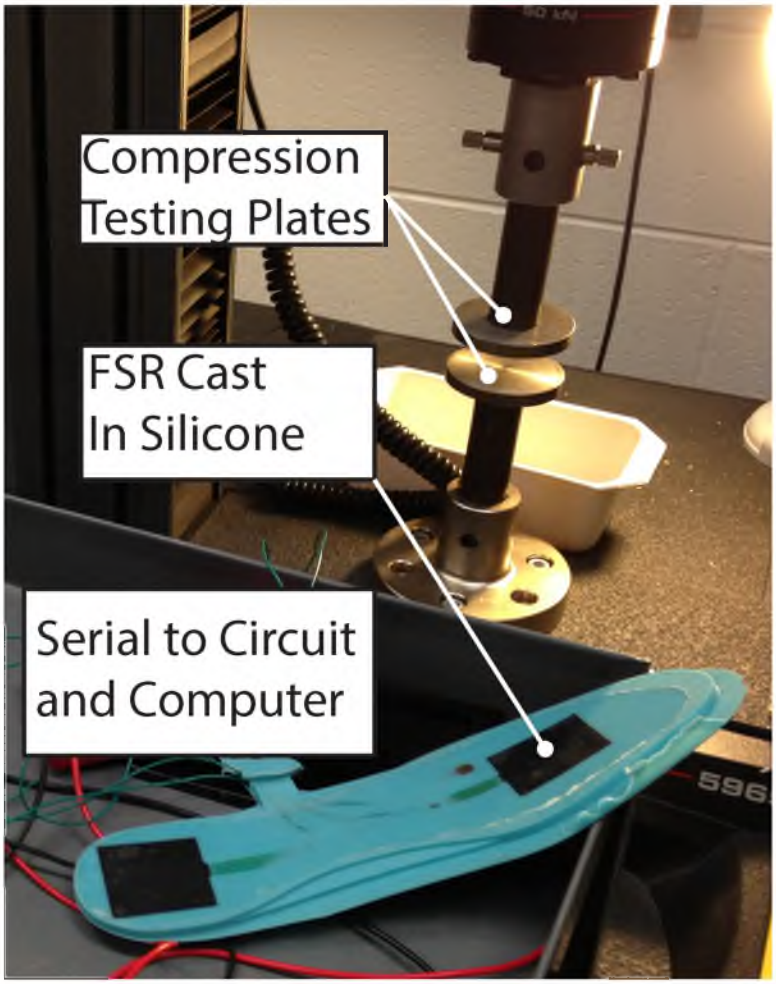

Figure 5.2: Compression Testing Environment for FSR modeling.
Notice the area of the compression testing plates were larger than the FSR. This difference required use of (5.3).

pressure of the compression disc was expressed as,

$$p = \frac{F_{comp}}{A_{disc}}, \tag{5.1}$$

and the pressure for the FSR is expressed as,

$$p = \frac{F_{FSR}}{A_{FSR}}, \tag{5.2}$$

where F_{comp} and F_{FSR} are the original force recorded from the compression test machine, and the force experienced by the FSR, respectively; and A_{disc} and A_{FSR} are the areas of the compression machine disc and the FSR, respectively. Since these pressures were the same, (5.1) and (5.2) were equated, and

$$F_{FSR} = 0.33 \cdot F_{comp}. \tag{5.3}$$

So $A_{FSR}/A_{disc} = 0.33$. This conversion is expressed as converted weight in Fig. 5.3.

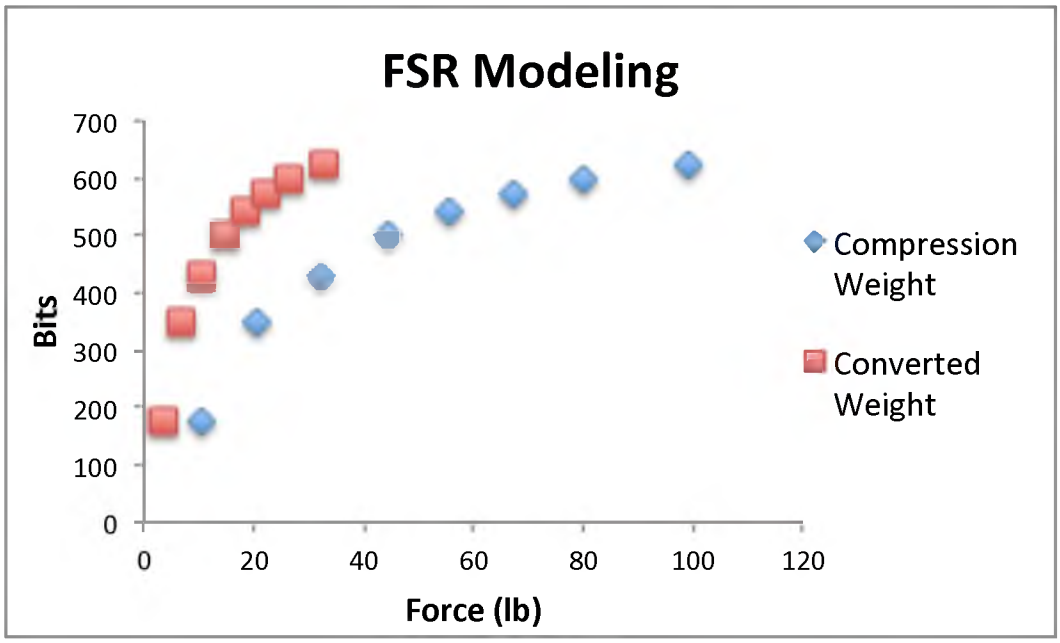

Figure 5.3: Data from FSR modeling. The compression weights were the original readings from the compression testing machine. The converted weight considered the difference in area between the FSR and the compression plates.

IMU Unit Conversion and Biasing

IMU data were recorded in bits (0 to 1023). The accelerometer was converted from bits to m/s^2 by multiplying by the manufacturer's specified scale factor of $9.81 \frac{\text{m}}{\text{s}^2} \frac{1}{256\text{bits}}$ to obtain traditional metric acceleration units. The gyroscope was converted from bits to $\frac{\text{rad}}{\text{s}}$ by dividing by a 14.375 scale factor, as specified by the manufacturer [11].

The IMU was oriented such that x, y, and z were aligned along the longitudinal, lateral/medial, and plantar directions, respectively, of the foot. Sensor bias drift is inherent in IMUs. This is especially a problem when collecting long periods of data. In prior human gait studies, regions of zero velocity, utilizing the stance time, were used to update the bias. In the skiing studies, the only guaranteed regions of zero velocity are at the very beginning and end of each trial. Understanding bias can by accomplished by separating the total measurements of linear acceleration and rotational velocity with the following equations:

$$\vec{a}_{meas} = \vec{a}_{trans} + \vec{a}_{bias} + \vec{a}_{grav} \tag{5.4}$$

and

$$\vec{\omega}_{meas} = \vec{\omega}_{rot} + \vec{\omega}_{bias}. \tag{5.5}$$

$\vec{a}$ and $\vec{\omega}$ are vectors that refer to linear acceleration and rotational velocity in the x, y, and z directions. The *meas* subscript refers to the measurement reported from the IMU, $\vec{a}_{trans}$ refers to the contribution of linear acceleration, $\vec{v}_{rot}$ refers to the contribution of rotational velocity, the *bias* subscript refers to the sensor bias, and $\vec{a}_{grav}$ refers to the contribution of gravity.

Since the trials generally took less than 90 seconds, the effects of $\vec{a}_{bias}$ and $\vec{\omega}_{bias}$ were negligible. Gravitational effects provide a significant contribution to the overall acceleration measurement, as illustrated in (5.4). For approximating the contribution due to gravity, it was assumed that x and y remained parallel and z remained normal to the slope. In other words, slow speed and utilization of beginning terrain helped ensure low angles of tilt (in the y-direction) of the feet with respect to the snow. This assumption simplified the analysis so that gravity was only considered in the x and z direction. Further, the gravity contribution was assumed to remain static.

Knowing the test course slope was measured at 6 degrees, this implied that the gravity contribution in the x-direction was approximately

$$a_{gravX} = g \sin 6^o, \tag{5.6}$$

where g was the constant gravitational acceleration. The gravity contribution in the z-direction was approximately

$$a_{gravZ} = g \cos 6^o. \tag{5.7}$$

A gravity constant of $g = 9.782\text{m/s}^2$ corresponded to the 8000 ft elevation of the test course. A small gravity contribution in the y-direction was likely present corresponding to edge angle, but was assumed to be insignificant.

Finding the bias was done iteratively by considering initial and final conditions. An offset corresponding to the noise bias was iteratively determined subject to the constraint of zero initial and final velocity. The accelerometer and gyroscope were both integrated once to obtain translational velocity and rotational position.

Understanding the initial and final conditions of zero velocity, (5.4) was numerically integrated to find the actual translational velocity as

$$\vec{v}_{actual} = \int \vec{a}_{trans} \mathrm{d}t. \tag{5.8}$$

Because all subjects begin from rest, these is no additional integration constant. The rotational position is found by a similar procedure using

$$\vec{\theta}_{actual} = \int \vec{\omega}_{rot} \mathrm{d}t, \tag{5.9}$$

Usable Data Set and Descriptive Statistics

At the beginning of each trial, test subjects were instructed to aggressively tap their foot twice. This created a data spike to identify when the subject was ready to begin. The data selected for the quantitative Potential to Fall (PF) analysis were taken from a window of acceptable data following these steps. This window was selected by investigating wedge and parallel data for all subjects to identify the number of consistent turns. The minimum across all subjects was six turns. To be consistent across all subjects, when analyzing PF, six turns were used.

The fastest and slowest trials through the 6 turns were 17.9 seconds and 44.0 seconds, respectively. The average and standard deviation for all the trials were 29.3 seconds and 9.0 seconds, respectively. Of the 9 data subjects used, 4 were female and 5 were male. Subject weight ranged from 135 lb to 200 lb. Subject height ranged from 5 feet 5 inches to 6 feet 2 inches.

Potential to Fall Metric

Every subject included in the PF analysis was required to have two acceptable WS and PS trials (four total). Nine of twelve subjects completed all trails successfully and were used in the PF analysis.

This metric is based on prior walking PF studies ([12] and Chapter 3) where normal and unexpected slipping gaits were compared. The original walking study identified a quantifiable PF metric, which compared normal to unexpected slip. This metric helped quantify repeatability between trials. More repeatable trials had a lower PF while less repeatable trails had a higher PF. The PF metric was based on comparing trials using Root Mean Squared Error (RMSE). While both the PF for skiing and PF for walking metrics used RMSE, skiing studies do not have a standard normal locomotion. Therefore, calculation of PF for skiing is slightly different. However, the calculation of RMSE is similar.

For every skiing subject, first WS and PS averages were computed for their two corresponding trials. Second, a RMSE was calculated between WS trials and WS average,

$$W_iW_ARMSE = \frac{\sum_{j=1}^{n_{short}} \sqrt{(W_{ij} - W_{Aj})^2}}{n_{short}}, \tag{5.10}$$

and PS trials and PS average,

$$P_iP_ARMSE = \frac{\sum_{j=1}^{n_{short}} \sqrt{(P_{ij} - P_{Aj})^2}}{n_{short}}. \tag{5.11}$$

This helped to quantify repeatability between WS and PS trials. The subscript $i = 1, 2$ indicates whether trial 1 or 2 was used, the subscript A denotes an average, W refers to WS, P refers to PS, and n_{short} refers to the number of terms in the dataset (as dictated by the shortest dataset of all the trials).

The PFS metric combined RMSE of gyroscope-x (edging), gyroscope-z (rotary), and FSR COP measurements. Both (5.11) and (5.10) were calculated three times to account for the three data sources. Then, each data source was normalized by finding the maximum of each of the trials,

$$RMSE_{max} = \max(P_iP_ARMSE, W_iW_ARMSE) \tag{5.12}$$

and then dividing (5.11) and (5.10) to normalize the RMSE,

$$W_iW_ARMSE_{norm} = \frac{W_iW_A}{RMSE_{max}}, \tag{5.13}$$

$$P_iP_ARMSE_{norm} = \frac{P_iP_A}{RMSE_{max}}. \tag{5.14}$$

Normalizing allowed all three RMSE values to be combined into a PFS metric as follows,

$$W_iW_{APFS} = W_iW_ARMSE_{norm_{gyroX}} + W_iW_ARMSE_{norm_{gyroZ}} + W_iW_ARMSE_{norm_{COP}} \tag{5.15}$$

$$P_iP_{APFS} = P_iP_ARMSE_{norm_{gyroX}} + P_iP_ARMSE_{norm_{gyroZ}} + P_iP_ARMSE_{norm_{COP}}. \tag{5.16}$$

where W_iW_{APFS} and P_iP_{APFS} are the PFS metric for WS and PS, respectively. Comparing the PFS from (5.15) and (5.16) quantifies whether WS or PS has a lower likelihood of falling.

Results and Discussion

Accelerometer

Translational acceleration and corresponding velocity, found using numerical integration, are illustrated for a sample subject, one of the expert skiers, in Fig. 5.4. PS is illustrated here, but WS is quite similar.

From the testing constraints, x and y velocity should start from zero, speed up semilinearly, periodically speed up and slow down (to maintain speed control), and then slow down semilinearly back to zero. Bias was adjusted were to satisfy the

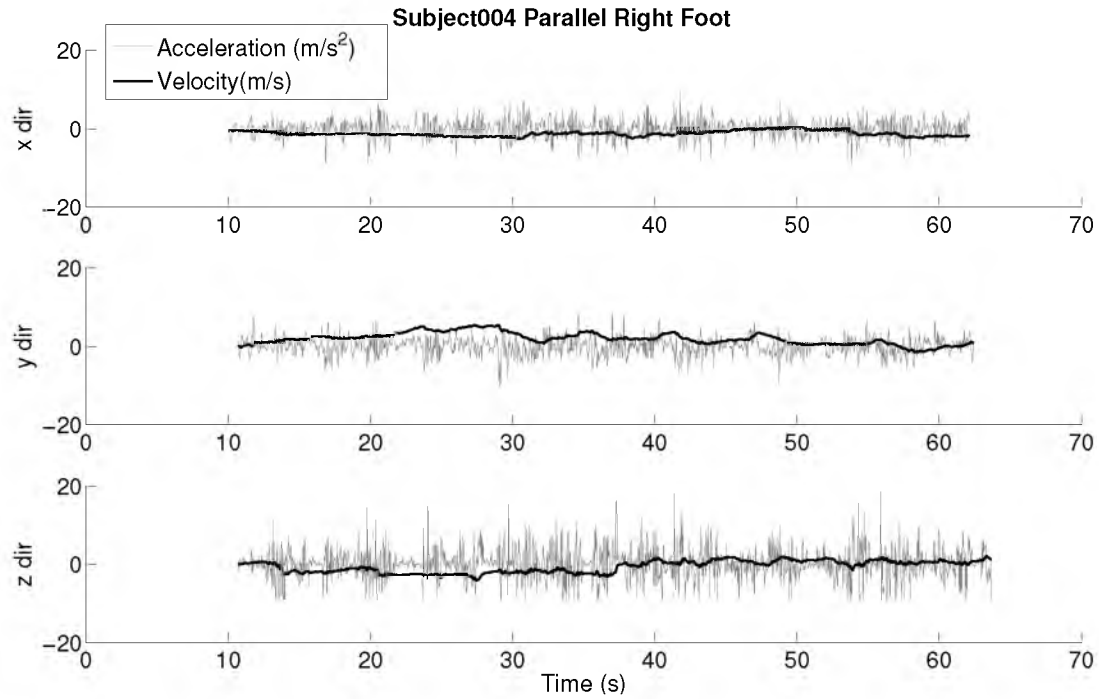

Figure 5.4: Sample Parallel Accelerometer Data.
Bias was adjusted such that velocity started and ended at zero. The stochastic patterns data shown by the figure were unusable in determining the likelihood of falling.

zero velocity endpoints. Prior work indicated that periodic motion led to lower likelihood of falling. When compared to the FSRs and the gyroscope, all axes of the accelerometer produced far more stochastic behavior.

Gyroscope

Rotational velocity and corresponding rotational position, found using numerical integration, are illustrated for the same expert subject in Fig. 5.5, 5.6, and 5.7. The x-axis measures ski edge tilt (edging), and the z-axis measures steering of the foot relative to the surface of the snow (rotary). Periodic locomotion is most obvious with rotary motion, which was used to identify the locations of the turning markers. This is done by identifying when the z-axis velocity equals zero, which indicates points of inflection (the transition between right-to-left or left-to-right turns) on the skier's paths. As illustrated by Fig. 5.8, each marker coincides with the apex of each turn,

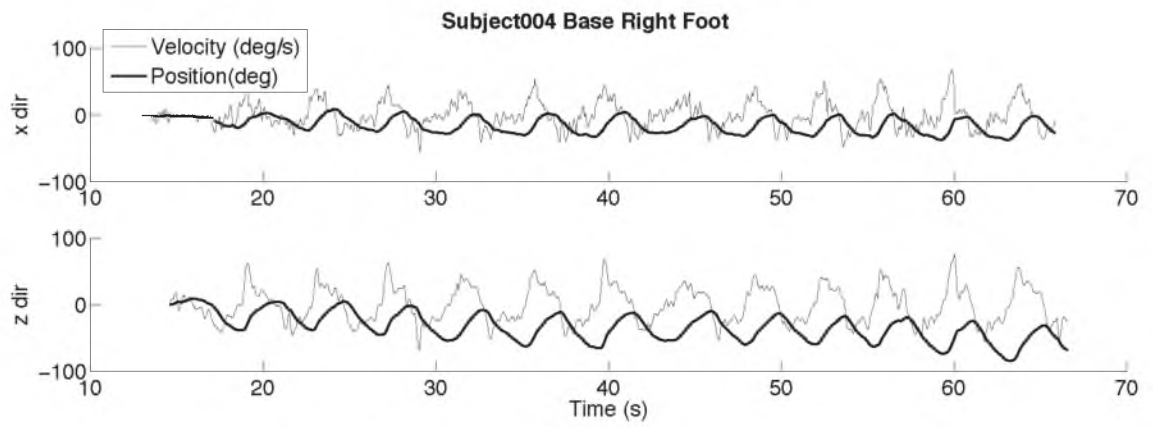

Figure 5.5: Sample baseline gyroscope data.

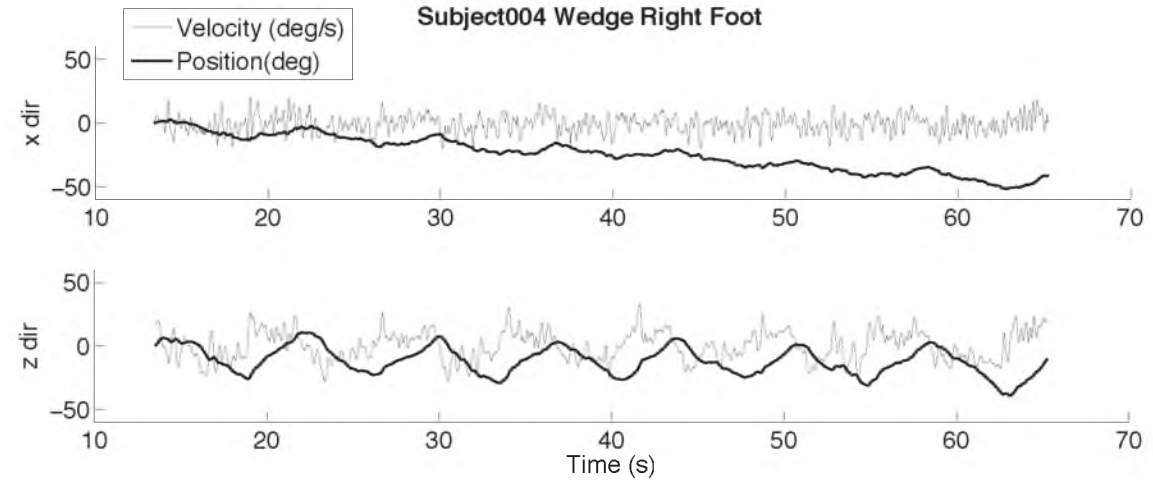

Figure 5.6: Sample WS gyroscope data.

which implies the point of inflection must be approximiately halfway between each marker.

For this particular subject, rotation about the x-axis is similar for baseline and PS skiing. This suggests the subject was using PS as their natural (baseline) skiing style. Rotations about both x- and z-axes suggest that the skier uses edging and rotary to provide turning, which according to the Professional Ski Instructors of America (PSIA) are fundamental turning movements [13]. Due to fore/aft rotational constraints, from the ski boot, y-axis rotation was easily corrupted by noise and produced inconclusive results, and was not included in this analysis.

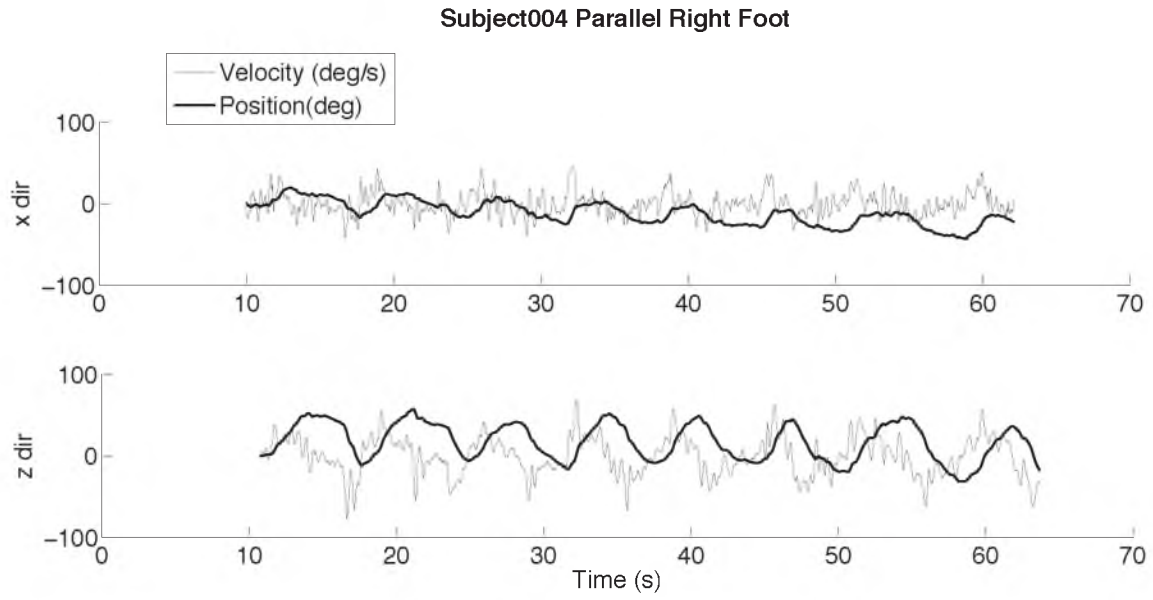

Figure 5.7: Sample PS gyroscope data.

WS shows similar behavior about the z-axis, but much smaller rotations about the x-axis, which suggest that WS relies much more on rotary opposed to edging to provide turning. Edging is known to be a more difficult skill, corresponding to PS being a more advanced technique. The small edging rotations permit excess noise that dominates the signal, leading to excessive drift.

FSR and COP

Similar to the gyroscope, the COP also produces the qualitative periodic behavior. Consider the same expert skier's baseline, WS, and PS toe and heel pressure, shown by Fig. 5.9, 5.10, and 5.11. The FSR calibration value is shown with the thick dashed line. For this particular subject, it is difficult to tell whether PS or WS has higher periodicity. It even appears that the skier's baseline skiing illustrates the most periodic motion. Subject 010, also an expert, illustrated similar trends as subject 004. Qualitatively, most skiers from this test illustrate the greatest periodic motion with WS locomotion.

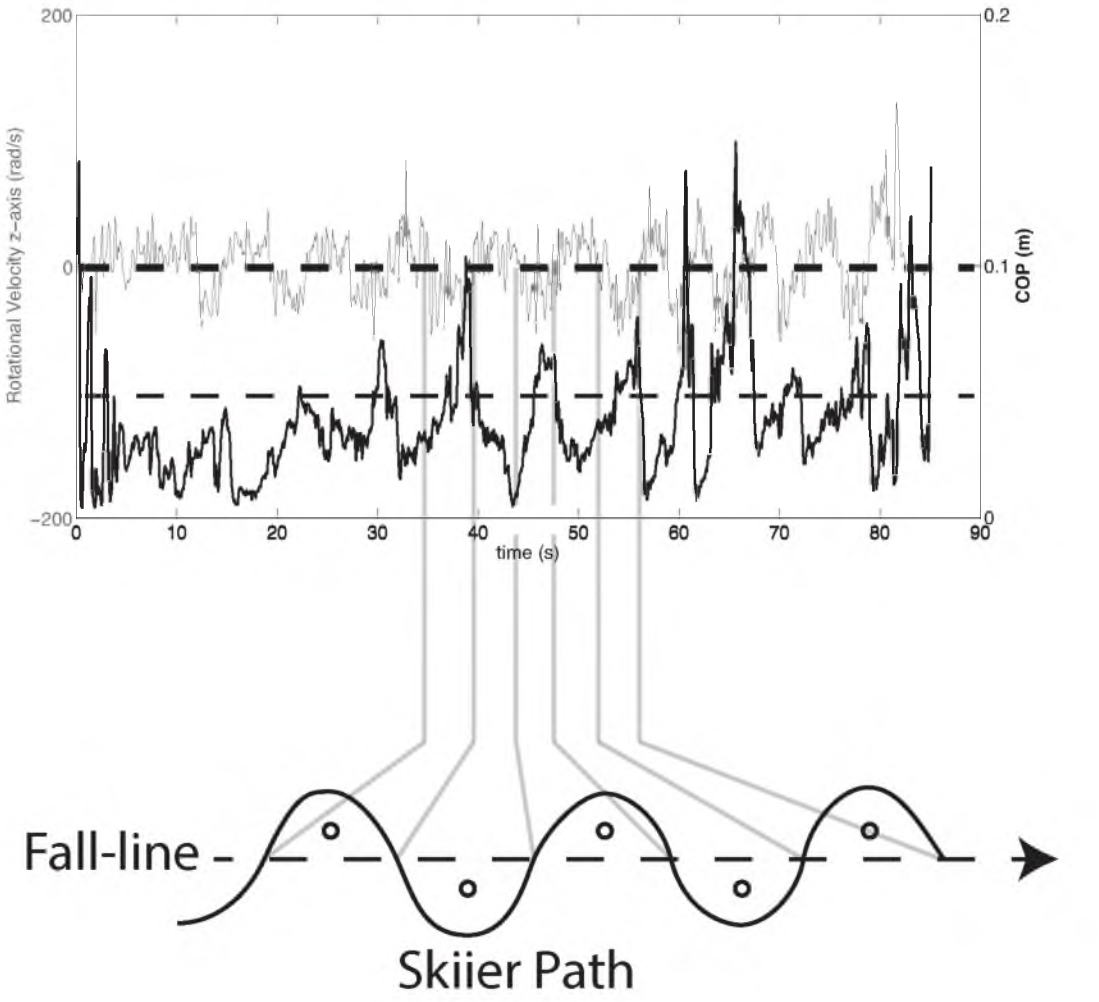

Figure 5.8: Link between markers, the gyroscope, and the FSRs.
Turn shape is indicated where the angular speed about the z-axis transitions between positive and negative.

Linking Turns with the Gyroscope and FSRs

In addition to rotary movement corresponding to turning markers, Fig. 5.8 also compares this relationship to the toe FSR to better understand how pressure management coordinates with turn shape. In addition to demonstrating rotary motion, the points of inflection on the path also correspond closely with the average, or neutral, value of the FSR. This suggests that forward pressure management is also

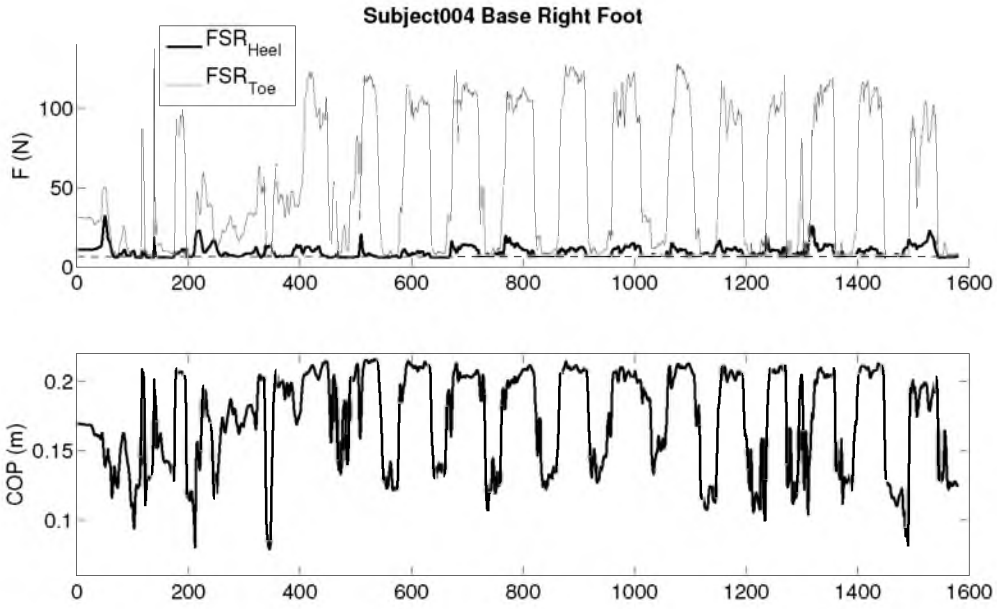

Figure 5.9: Subject 4 baseline.
Front and Rear FSRs values are given in the top subfigure.

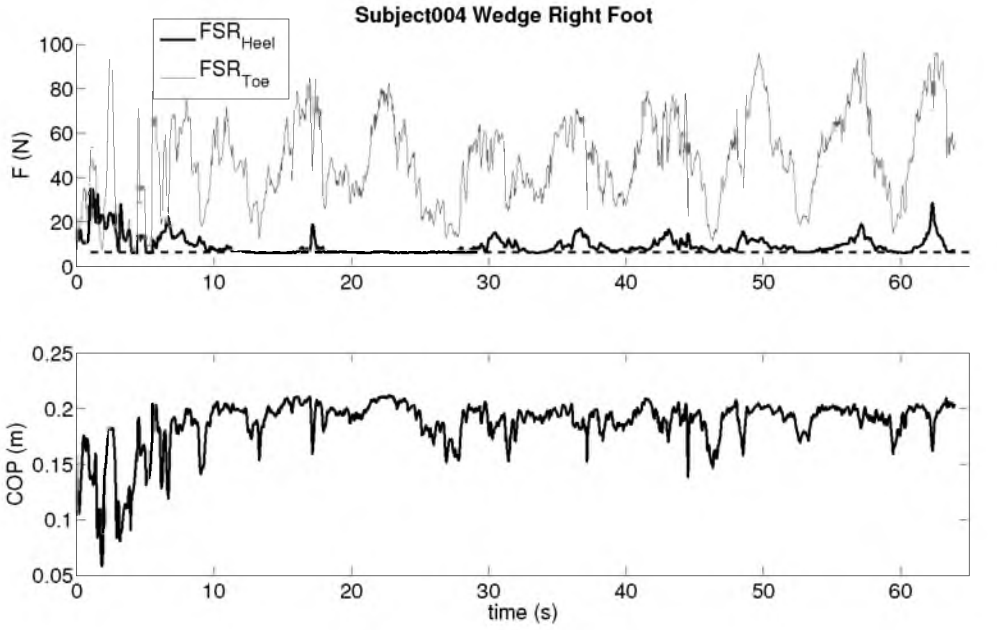

Figure 5.10: Subject 4 wedge COP.
Front and Rear FSRs values are given in the top subfigure.

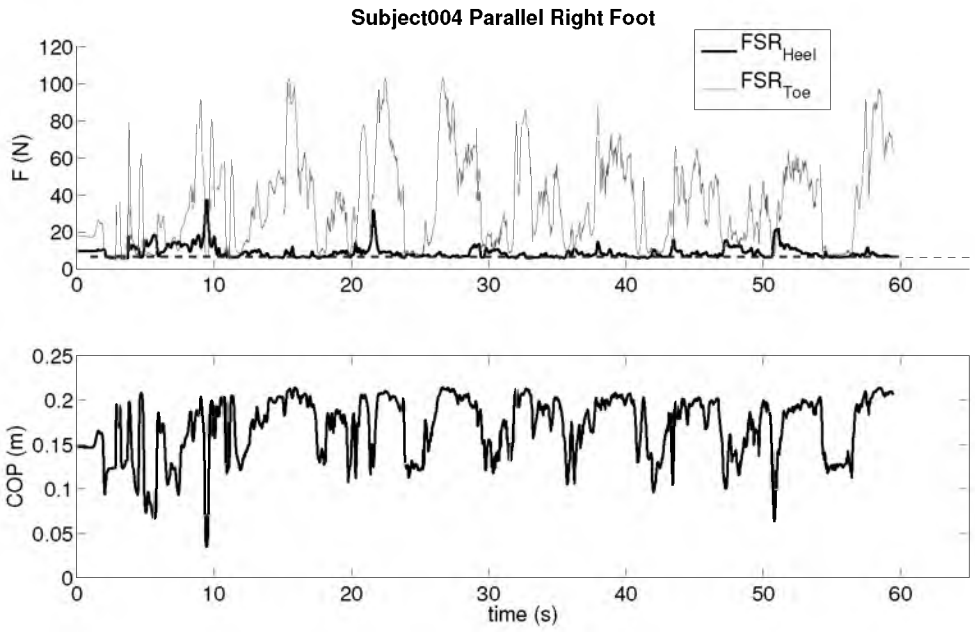

Figure 5.11: Subject 4 parallel COP.
Front and Rear FSRs values are given in the top subfigure.

a key factor to turn initiation. In addition to edging and rotary as key components in turn creation, as presented in Fig. 5.5, 5.7, and 5.6, pressure management can also be considered a key component of turn creation. Rotary, edging, and pressure are all key components in proper skiing technique, as confirmed by PSIA [13].

RMSE

RMSE comparisons, using z-axis gyroscope data, of WS and PS are shown in Fig. 5.12 and 5.13. Fig. 5.12 focuses on 1 expert subject while Fig. 5.13 focuses on 1 intermediate subject. When compared to PS RMSE, WS RMSE of both the intermediate and expert subjects were closer to zero. The lower WS RMSE, which were similar for all subjects, suggested that WS was more repeatable than PS. Combining the RMSE (using the x- and z-axis gyroscope and COP) of all subjects is illustrated using the PF metric as presented in the next section.

Potential to Fall

Fig. 5.14 and Fig. 5.15 show PF for intermediate and expert subjects. For all subjects, the RMSE of WS trials are smaller than PS. This explains why all the

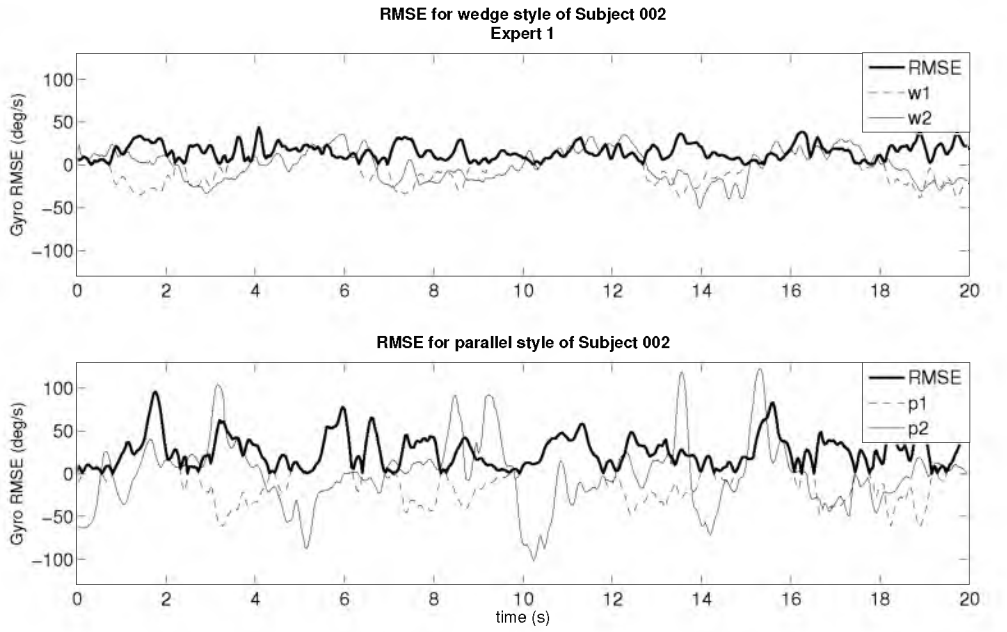

Figure 5.12: Gyroscope RMSE for Expert Subject 1.

parallel PF metrics for the gyroscope in the x and z directions, and most of the COP, are equal to one.

Edging and rotary measurements (from gyroscope-x and z, respectively) produce a clearly greater RMSE when comparing parallel to wedge. Although suggested, conclusive RMSE results based on COP can not be made. However, 1/5 intermediates, compared to 3/4 experts, showed a significantly lower PF. These results suggest that the expert skiers are more capable of using pressure management to decrease the potential to fall. This suggests that pressure management is a more advanced skill, and that it is more lacking in intermediate skiers.

When combining the gyro and COP RMSE data to form the PF metric, as done in Fig. 5.14 and 5.15, the PF is always smaller for the wedge compared to parallel.

Future Work

This work is just the beginning of a much greater area of research. Even though the gyroscope produced excellent results, 3D data processing would give a much more accurate correlation between all degrees of freedom of the IMU. Although 3D IMU

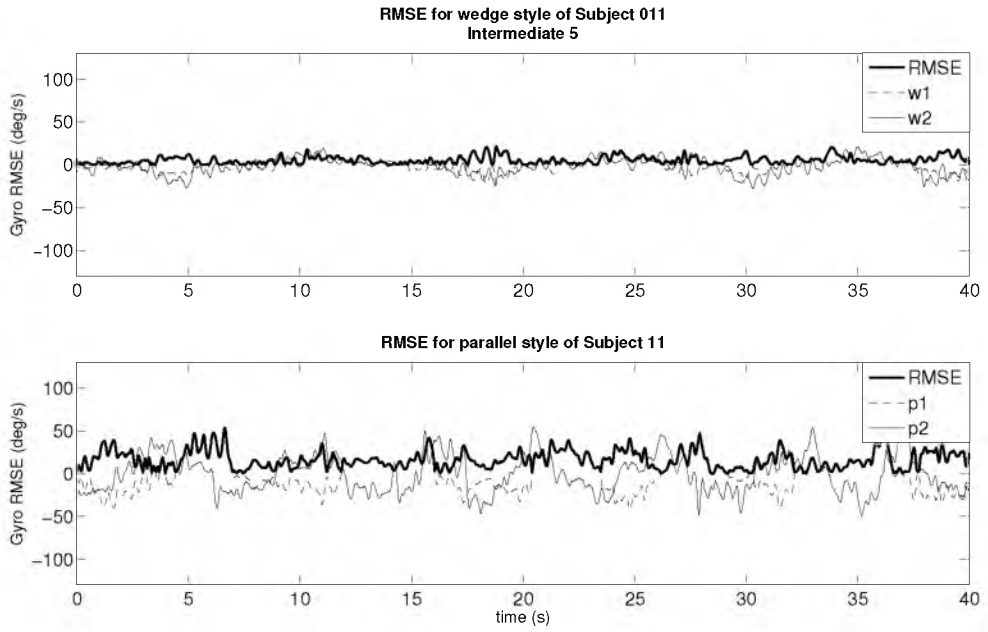

Figure 5.13: Gyro RMSE for subject 11 (Intermediate subject 5).

implementation can be quite involved, as shown by Johnson [14], this would deliver more accurate analysis of the complex motion of the feet during skiing locomotion.

One of the greatest challenges was correlating similar stages of locomotion between trials. Advanced IMU analysis would allow for complete turn shape information and provide better matching of trials. While the basic approach here to match periodic motion did enable analysis of skiing locomotion, automating would likely produce even better results. Clearer turn shapes, from an advanced IMU implementation, would better allow us to study WS versus PS turn by turn rather than fixing a window of time.

Refining these tools would permit testing on larger courses with variations in terrain. One of the challenges in this analysis was no subjects experienced a fall, so this analysis is based on inconsistency between trails. The goal would be to extend the study, e.g., to monitor skiing throughout an entire day, such that falls would safely be experienced and detectible.

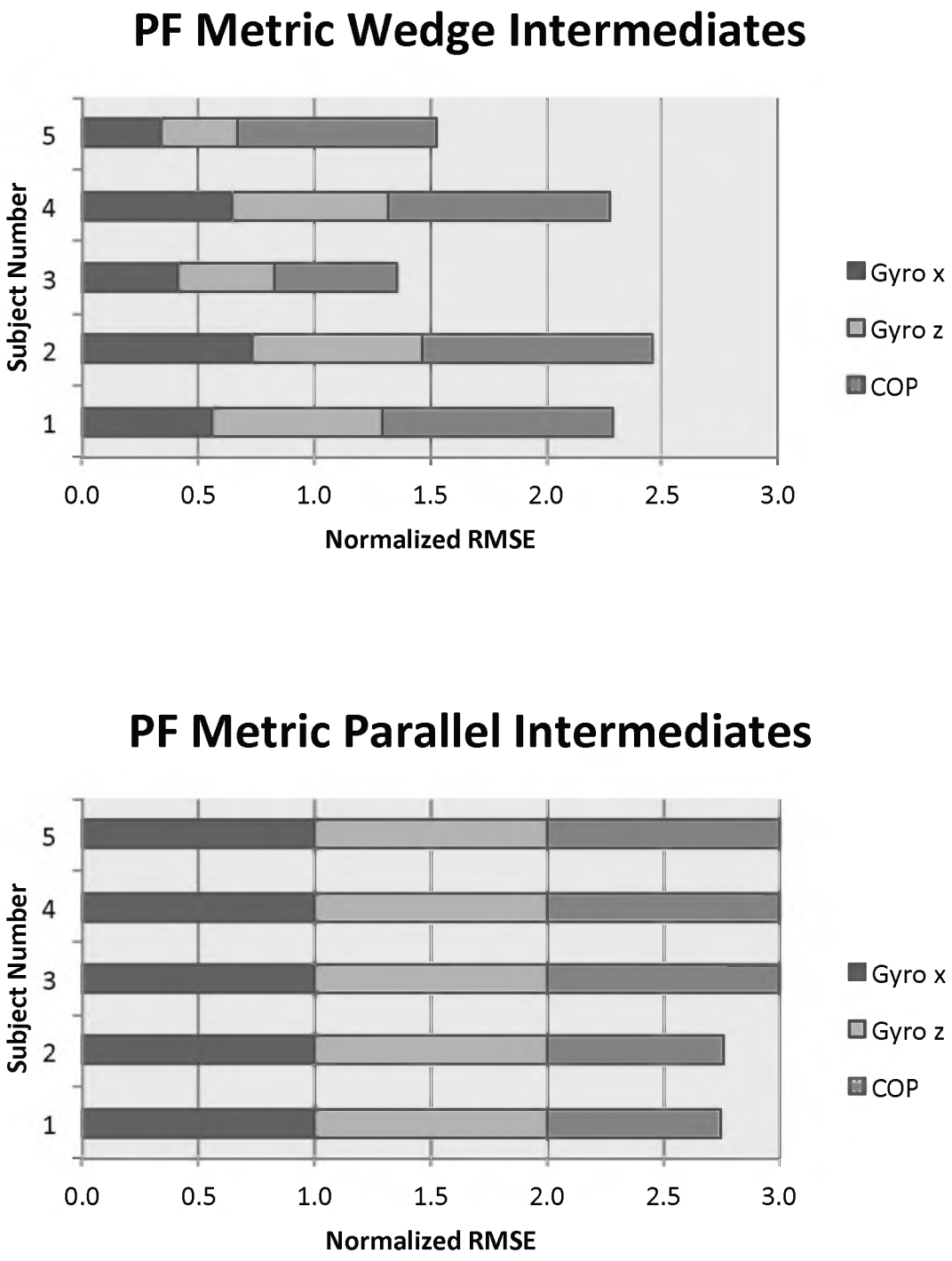

Figure 5.14: PF metric for intermediate skiers.
For every intermediate subject, the total PF (including the x- and z-axis gyroscope and COP) is less for WS than PS.

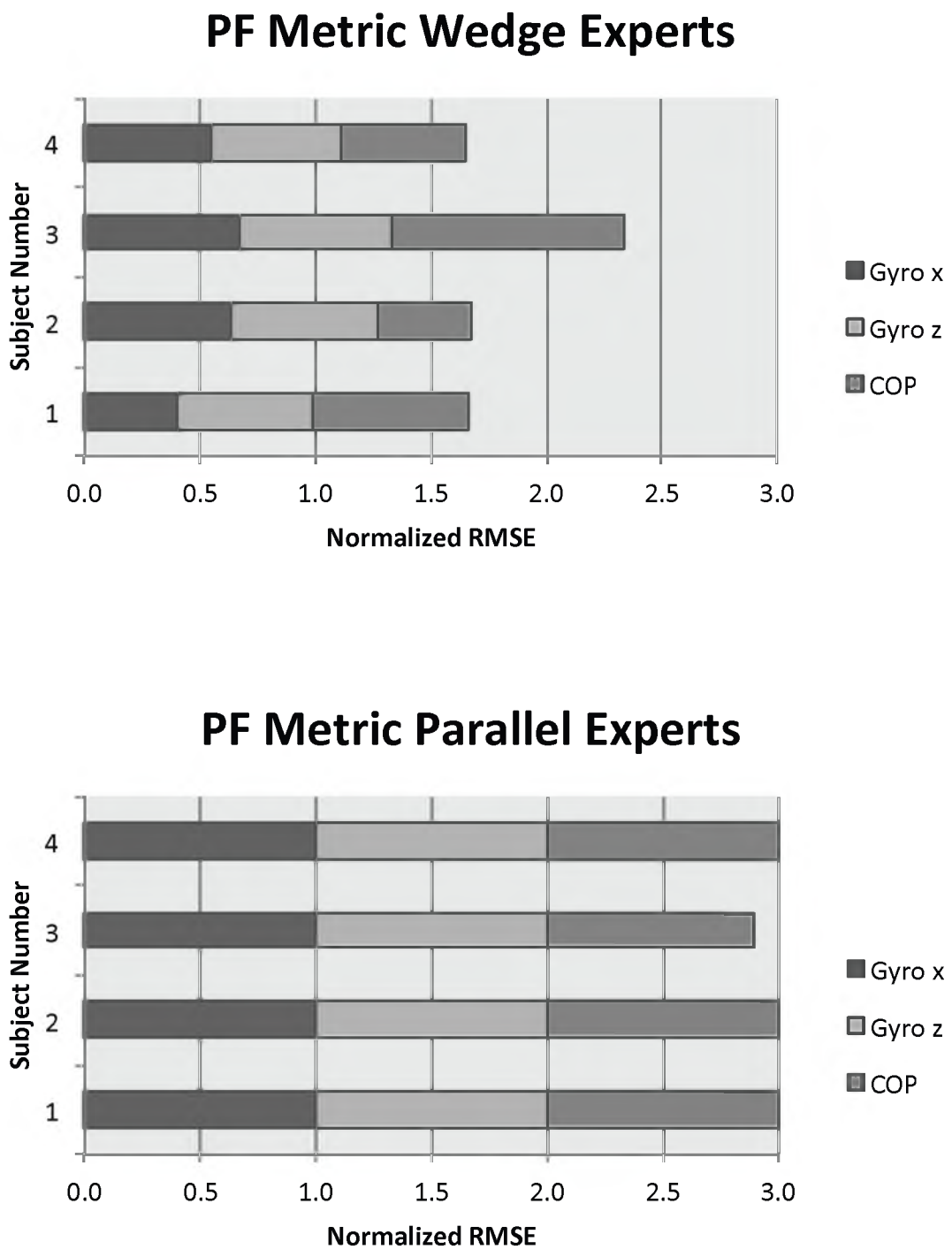

Figure 5.15: PF metric for expert skiers.
Like the intermediate subjects, the total PF (including the x- and z-axis gyroscope and COP) of the expert subjects is less for WS than PS.

Conclusion

This paper analyzed Potential to Fall for Skiers (PFS) using an instrumented insole mounted in a ski boot. The insole contained a 6-Degree Of Freedom Inertial Measurement Unit (IMU) and toe and heel mounted Force Sensitive Resistors (FSRs). Both were used to investigate Potential to Fall. The FSRs were also used to calculate Center of Pressure (COP), which was used to formally calculate a metric to determine PFS. The PFS metric correlates extremely well to prior work on walking studies.

References

[1] C. Redd and S. Bamberg, "A wireless sensory feedback system for real-time gait modification," in *Engineering in Medicine and Biology Society, EMBC, 2011 Annual International Conference of the IEEE.* IEEE, 2011, pp. 1507–1510.

[2] S. J. M. Bamberg, P. LaStayo, L. Dibble, J. Musselman, and S. Raghavendra, "Development of a quantitative in-shoe measurement system for assessing balance: Sixteen-sensor insoles," *IEEE EMBC*, 2006.

[3] S. J. M. Bamberg, P. Dyer, L. Lincoln, and L. Yang, "Just enough measurement: A proposed paradigm for designing medial instrumentation," *IEEE EMBC*, 2011.

[4] P. Dyer and B. S. J. M. and, "Instrumented insole vs. force plate: A comparison of center of plantar pressure," *IEEE EMBC*, 2011.

[5] A. Johnson, "Development and testing of a gait estimation system," Master's thesis, The University of Utah, 2012.

[6] A. Kourepenis, J. Borenstein, J. Connelly, R. Elliott, P. Ward, and M. Weinberg, "Performance of mems inertial sensors," in *Position Location and Navigation Symposium, IEEE 1998.* IEEE, 1998, pp. 1–8.

[7] B. S. Davis, "Using low-cost mems accelerometers and gyroscopes as strapdown imus on rolling projectiles," in *Position Location and Navigation Symposium, IEEE 1998.* IEEE, 1998, pp. 594–601.

[8] J. Chen, K. Kwong, D. Chang, J. Luk, and R. Bajcsy, "Wearable sensors for reliable fall detection," in *Engineering in Medicine and Biology Society, 2005. IEEE-EMBS 2005. 27th Annual International Conference of the.* IEEE, 2006, pp. 3551–3554.

[9] A. Bourke and G. Lyons, "A threshold-based fall-detection algorithm using a bi-axial gyroscope sensor," *Medical engineering & physics*, vol. 30, no. 1, pp. 84–90, 2008.

[10] M. Bächlin and G. Tröster, "Swimming performance and technique evaluation with wearable acceleration sensors," *Pervasive and Mobile Computing*, vol. 8, no. 1, pp. 68–81, 2012.

[11] "Itg-3200 product specification," Spark Fun Electronics, Tech. Rep., 2010.

[12] A. Vogt, A. Merryweather, K. Beschorner, and S. J. M. Bamberg, "Potential to fall of bipeds using foot kinematics," in *International Conference of the IEEE Engineering in Medicine and Biology Society (EMBC) Conference 2013, Osaka, Japan*, 2013.

[13] *Alpine Technical Manual: Skiing And Teaching Skills.* Professional Ski Instructors of America, 2002.

[14] E. Johnson, "Investigating inertial measurement for human-scale motion tracking," Ph.D. dissertation, The University of Utah, 2011.

CHAPTER 6

CONCLUSION

This thesis undertook an in-depth analysis of bipedal stability by analyzing the likelihood of falling and applying a Potential to Fall (PF) metric based on Root Mean Squared Error (RMSE). Both were generalized by using walking gaits and skiing locomotion.

The method of data collection used depended on the type of locomotion. For walking gaits, a motion capture laboratory with three-dimensional (3D) stereographic cameras and 6-Degree Of Freedom (DOF) force plates was used. This worked well because the environment was easily recreated in a lab. In contrast, instrumented insoles were used for skiing locomotion because the environment could not effectively be recreated in a lab.

The research hypothesis was that *Center of Pressure (COP) and kinematic marker trajectories change as the likelihood of falling changes in human walking gait and human skiing gait.* Using two aims, we were able to prove this hypothesis:

- Aim 1: Walking likelihood of falling is understood using kinematic hip and foot markers and kinetic changes in COP under each foot.
- Aim 2: Skiing likelihood of falling is understood using kinematic foot markers and the change in COP under each foot.

Walking likelihood of falling was shown with hip, foot, and sternum markers kinematics as well as COP. When conducting multiple trials, it was found that an unexpected slip caused rapid changes in kinematics. With a normal gait, these kinematics were periodic; however, the slipping made it nearly impossible to repeat the periodic trends and this was an indication of an elevated likelihood of falling. This study suggested that both hips and feet illustrate this behavior, implying either

can be used to analyze the likelihood of falling. The COP also reflected the base of support, and showed how the upper body moved with respect to the lower body. With increased likelihood of falling, the COP covered a much larger range.

A PF metric was developed using foot kinematics for a group of subjects. The PF metric is based on the assumption that repeatable gait reflects low likelihood of falling. Repeatability is identified using RMSE between trials. RMSE of various trials were plotted in an x-y graph. Then a trend line was fitted to the data and the slope and y-intercept of the tend lines were used as indicators of PF. Based on the PF metric, the normal gait showed high repeatability and unexpected slipping gaits showed low repeatability.

The likelihood of falling of skiers had to be approached differently primarily because slip is inherent in skiing. The skiing studies compared Wedge Style (WS) to Parallel Style (PS) skiing. As in walking, it was hypothesized that when comparing two types of locomotion, WS and PS in this case, that one would be more repeatable and lead to a lower likelihood of falling. Unlike PS, WS, which is one of the first styles used by beginning skiers, had a much larger base of support and involves less complicated locomotion. Results from a pilot study, based on COP measurements, refined the hypothesis that WS led to lower likelihood of falling because of greater periodic trends when comparing to PS.

The connections made with walking studies supported using only kinematics of the foot, instead of the upper body, to determine likelihood of falling. Like walking studies, skiing likelihood of falling was illustrated using periodic repeatability of locomotion. This was important because it allowed use of inexpensive foot sensors without the need of an upper body sensor. The skiing studies based likelihood of falling on angular kinematics, rotary and edging movements, and COP.

When developing a quantitative Potential to Fall while skiing metric, based on RMSE, the accelerometer, gyroscope, and COP where tested. While the accelerometer produced inconclusive results, edging and rotary ankle rotations (measured by two independent axes of the gyroscope) indicated that WS had a lower PF than PS. COP but did now produce results as convincing as the gyroscope. 3/4 experts, compared to 1/5 intermediate subjects, produced a convincing lower PF that did help

to indicate that understanding does lower the likelihood of falling, but is an advanced skill. However, combining edging, rotary, and COP unanimously illustrates for both intermediates and experts that WS has a lower PF than PS. Using edging, rotary, and COP management was consistent with standards of good skiing technique by the Professional Ski Instructors of America.

There are many possible future extensions to this work. While the 2D IMU implementation was successful, 3D IMU analysis would help further develop the PF metic for skiing. 3D IMU would permit a better identification of turn shape and a more accurate comparison between repeatability between trials.

All tests were conducted on beginner level terrain, but this work would be more comprehensive on terrain with more variations (including obstacles, slope, and snow conditions). However, this requires tools that allow for longer periods of testing with less invasive instrumentation. A natural solution is to use smart phones. They provide a user-friendly interface, have accessible built-in IMUs, and provide data acquisition. Smart phones also provide greater engineering and educational potential by allowing the users to get instantaneous feedback. In this thesis, assumptions had to be made between the implications of balance and falling, because no falls occurred. Providing more time for data collection on more challenging terrain would allow falls to occur and lead to more definite conclusions.

Additional steps to improving scientific fundamentals for likelihood of falling and the PF metric could be accomplished through studying more modes of human locomotion. This includes locomotions not studied in this thesis (e.g., biking, running, jumping, etc.), but it also includes looking at walking in the nonlaboratory study. A nonlaboratory setting provides some of the critical elements leading to a loss of balance, which simply cannot be simulated in a laboratory.